

THE STELLAR MASS CONTENT OF SUBMILLIMETER-SELECTED GALAXIES

LAURA J. HAINLINE^{1,2}, A. W. BLAIN^{3,4}, IAN SMAIL⁵, D. M. ALEXANDER⁶, L. ARMUS⁷, S. C. CHAPMAN⁸, AND R. J. IVISON^{9,10}

Draft version April 2, 2024

ABSTRACT

We present a new study of stellar mass in a sample of ~ 70 submillimeter-selected galaxies (SMGs) with accurate spectroscopic redshifts. We fit combinations of stellar population synthesis models and power laws to the galaxies' observed-frame optical through mid-IR spectral energy distributions to separate stellar emission from non-stellar near-IR continuum. The availability of spectroscopic redshifts significantly enhances our ability to determine unambiguously not only the mass and luminosity of SMGs, but also the presence and contribution of non-stellar emission to their spectral energy distributions. By separating the stellar emission from the non-stellar near-IR continuum, we find that $\sim 50\%$ of our sample have non-stellar contributions of less than 10% in rest-frame H -band and $\sim 10\%$ of our sample have non-stellar contributions greater than 50%. We find that the K -band luminosity of the non-stellar continuum emission is correlated with hard X-ray luminosity, indicating an AGN origin of the emission. Upon subtracting this AGN-contributed continuum component from all of the galaxies in our sample, we determine a lower median stellar mass for SMGs than previous studies, $\sim 7 \times 10^{10} M_{\odot}$. We use constraints of the starburst time-scale from molecular gas studies to estimate the amount of fading our sample would undergo if they passively evolve after the starburst terminates. The results suggest that typical SMGs, while among the most massive galaxies at $z \sim 2$, are likely to produce descendants of similar mass and luminosity to L^* galaxies in the local universe.

Subject headings: galaxies: high redshift — galaxies: formation — galaxies: evolution — infrared: galaxies

1. INTRODUCTION

Soon after their discovery, the population of high- z , far-infrared (far-IR) luminous galaxies revealed in deep submillimeter surveys (e.g., Smail et al. 1997; Hughes et al. 1998; Barger et al. 1998; Eales et al. 1999) were proposed to represent the formation of (the most) massive, metal-rich spheroids (Lilly et al. 1999; Smail et al. 2002; Swinbank et al. 2006). Submillimeter-selected galaxies (SMGs) have thus tantalized observers as a potential opportunity to witness the formation of massive galaxies directly. The far-IR luminosities ($> 10^{12} L_{\odot}$; e.g., Chapman et al. 2005; Kovács et al. 2006; Magnelli et al. 2010; Chapman et al. 2010) of these dusty, gas-rich galaxies (e.g., Frayer et al. 1998; Greve et al. 2005) imply star formation rates in excess of $10^3 M_{\odot} \text{ yr}^{-1}$, sufficient to form the stellar mass of an L^* galaxy in $\sim 100 \text{ Myr}$, potentially explaining the seemingly uniformly-old stellar populations of local ellipticals (e.g., Bower et al. 1992; Kauffmann et al. 2003) and massive galaxy populations at $z \sim 1 - 3$ (e.g., Franx et al. 2003; Steidel et al.

2003; Glazebrook et al. 2004; Daddi et al. 2004). Moreover, the observed clustering of SMGs (Blain et al. 2004b; Weiß et al. 2009) is similar to that of massive galaxies in the local universe, and suggests that SMGs reside within $\sim 10^{13} M_{\odot}$ dark halos. Yet, the formation of such massive galaxies on such rapid time-scales is difficult to account for using theoretical models of galaxy formation (e.g., Guiderdoni et al. 1998; Devriendt & Guiderdoni 2000; Baugh et al. 2005; Swinbank et al. 2008).

Determining the masses of high- z SMGs, especially the stellar and gas masses, and their relationship to other populations of high- z galaxies is thus crucial to understanding the link between SMGs and massive galaxies in the local Universe and places much-needed constraints on the $z = 0$ descendants of SMGs. Prior to the advent of the *Spitzer Space Telescope*, however, constraints on the stellar mass were difficult to obtain for SMGs, especially for individual galaxies, due to significant obscuration at optical and near-IR wavelengths (rest-frame UV and optical; see Smail et al. 2004; Swinbank et al. 2004; Pope et al. 2005). The rest-frame near-infrared (near-IR), which *Spitzer* gives us the power to probe for high- z galaxies, is less affected by reddening than optical-band data, and thus is beneficial when looking at SMGs which suffer from extinction in the rest-frame UV and optical bands. In addition, because the near-IR luminosity is much less dependent on past star formation history than, for example, the optical-band luminosity (e.g., Kauffmann & Charlot 1998), the rest-frame near-IR continuum emission permits the best determination of total stellar mass in both young and old stars.

Using data from *Spitzer*-IRAC, Borys et al. (2005), Hainline (2008), Dye et al. (2008), and Michałowski et al. (2010) have all calculated stellar masses for individual SMGs by fitting the observed-frame optical through mid-IR spectral energy distributions (SEDs), obtaining typical stellar masses ranging from $10^{10.8} - 10^{11.8} M_{\odot}$; Hainline (2008), Dye et al. (2008), and Michałowski et al. (2010) also find evidence of

¹ Dept. of Physics, United States Naval Academy, 572C Holloway Rd, Annapolis, MD 21402, USA; hainline@usna.edu

² Dept. of Astronomy, University of Maryland, College Park, MD 20742, USA

³ Dept. of Physics and Astronomy, University of Leicester, University Road, Leicester LE1 7RH, UK

⁴ Dept. of Astronomy, California Institute of Technology, Mail Code 249-17, Pasadena, CA 91125, USA

⁵ Institute for Computational Cosmology, Durham University, South Road, Durham DH1 3LE, UK

⁶ Dept. of Physics, Durham University, Durham DH1 3LE, UK

⁷ Spitzer Science Center, California Institute of Technology, Mail Code 220-6, Pasadena, CA 91125, USA

⁸ Institute of Astronomy, University of Cambridge, Madingley Road, Cambridge CB3 0HA, UK

⁹ Institute for Astronomy, University of Edinburgh, Blackford Hill, Edinburgh EH9 3HJ, UK

¹⁰ UK Astronomy Technology Centre, Royal Observatory, Blackford Hill, Edinburgh EH9 3HJ, UK

significant stellar mass assembly prior to the SMG phase. However, none of the previous stellar mass studies addressed the contribution of near-IR continuum excess to the SEDs of SMGs, noted by Borys et al. (2005) and Hainline (2008) in numerous SMGs in their samples, which may represent very hot dust heated by AGN. Contamination of the stellar masses by AGN could especially be a problem for Borys et al. (2005), who used a small, X-ray-detected SMG sample which was thus possibly biased towards SMGs with stronger AGN contributions (or lower X-ray obscuration). While X-ray observations and mid-IR spectra of SMGs indicate that the majority of the population are not dominated by an active nucleus (AGN), many SMGs host AGN activity (Alexander et al. 2003, 2005; Pope et al. 2008; Menéndez-Delmestre et al. 2009), which may not be negligible for the purpose of stellar mass studies.

We have published a *Spitzer*-IRAC and MIPS survey of a sample of ~ 70 radio-detected SMGs with spectroscopic redshifts (Hainline et al. 2009, hereafter Paper I), a factor of 5 larger than the sample considered by Borys et al. (2005). In this paper we combine our IRAC data set from Paper I with optical and near-IR photometry from the literature to analyze the rest-frame UV to near-IR SEDs of the sample to determine stellar masses for these SMGs, while accounting for a contribution to the near-IR luminosity from hot, possibly AGN-heated, dust, expanding the analysis of Hainline (2008). With our large sample size, spectroscopic redshifts¹¹, and treatment of non-stellar emission, we can make estimates of SMG stellar mass which better represent the stellar component than those estimates currently available from Borys et al. (2005) and Michałowski et al. (2010). Using our new estimates, we can evaluate whether SMGs contain enough mass to represent the formation of the most massive galaxies and make predictions for SMG descendants.

The structure of the paper is as follows: we begin in §2, describing our SMG sample and data. In §3 we discuss the methods we use to determine stellar masses for our sample. In §4 we present our results from the fits of the stellar population models to the observed SEDs. In §5 we conduct independent checks on the stellar masses from dynamical masses obtained through observations of CO rotational transitions, with the caveat that the dynamical masses are also subject to systematic uncertainties arising from assumptions that the gas traces the total mass and the galaxies are in virial equilibrium, then compare the stellar masses of SMGs to those of other high- z galaxy populations, and conclude by discussing the evolution of SMGs to the present day. Throughout our analysis and discussion, we assume $\Omega_M = 0.27$, $\Omega_\Lambda = 0.73$, and $H_0 = 71 \text{ km s}^{-1} \text{ Mpc}^{-1}$ (Hinshaw et al. 2009).

2. OPTICAL, NEAR-IR, AND MID-IR DATA

In Paper I, we present *Spitzer*-IRAC measurements for the spectroscopic SMG sample from Chapman et al. (2005, C05 hereafter). Their final spectroscopic sample contains 73 SCUBA galaxies (median $S_{850} = 5.7 \pm 3.0 \text{ mJy}$), each of which was required to be detected in very deep (1σ noise $\sim 5\text{--}11 \mu\text{Jy}$), high-resolution ($\sim 1''$) Very Large Array (VLA) maps at 1.4 GHz to obtain a position accurate enough for optical spectroscopy. The redshift distribution of the C05 sample, when corrected for spectroscopic incompleteness, is well-

characterized by a Gaussian with median redshift of $z = 2.2$ and $\sigma_z = 0.8$. None of the $z > 1$ SMGs in the final sample analyzed in C05 are suspected to be strongly lensed. We refer the reader to C05 and Paper I for further details on the sample and *Spitzer* observations. We will exclude from our analysis 2 SMGs from the IRAC-observed subsample whose radio counterparts are in doubt (and which were not detected by *Spitzer*): SMM J131231.07+424609.0 and SMM J221725.97+001238.9. We also exclude from our analysis the galaxies which are suspected to be low- z lenses of background submillimeter sources in C05, as in C05 and Paper I. The final sample which we analyze in this paper thus contains 67 radio-detected SMGs, and includes the entire sample of 13 X-ray detected SMGs analyzed by Borys et al. (2005). We note that a bias towards emission-line galaxies is introduced into our sample since the SMGs are required to be spectroscopically-identified: the redshift of an emission-line galaxy is more easily identified than that of a galaxy without emission lines when the continuum flux is faint and has a low signal-to-noise ratio. While one obvious consequence of this bias is that our sample is incomplete in the “redshift desert” between $z \sim 1.2$ and $z \sim 1.8$, the bias may also result in preferential selection of galaxies which contain less-obscured star formation or AGN activity. In addition, since we require a radio detection of the galaxies in our sample in order to obtain the spectroscopic redshift, we may be selecting against SMGs with cold dust or higher redshift (see, e.g., Ivison et al. 2002; Eales et al. 2003; C05). As a result of these biases, the conclusions we draw must be restricted to apply only to spectroscopically identified, radio-detected SMGs. However, a wide range of luminosity and redshift is still probed within these selection limits (see, e.g., Ivison et al. 2002; Blain et al. 2004a).

Although we postpone a discussion of the uncertainties associated with our modeling procedure to later sections, we note that, in principle, to obtain the best constraints on the stellar population ages and the extinction of starlight from fitting stellar population models to the SEDs of high- z galaxies, we must use photometry which spans the 4000 Å break and the rest-frame UV through optical bands, respectively (e.g., Shapley et al. 2001, 2005). Thus, for our present study we combine observed-frame optical and near-IR measurements from a variety of literature sources with our IRAC measurements presented in Paper I to obtain the most wavelength coverage possible. The available observed-frame optical photometric bands vary for each of the seven sky fields in our sample; see §3.3 for a discussion of the impact on our final results of the varying number of photometric constraints within the galaxy sample. In Table 1 we summarize for each field the photometric bands available and the typical number of optical and near-IR photometric constraints per galaxy. For the CFRS-03h field, we use here UBV data from Clements et al. (2004) and R data from C05. For the Lockman East field, we use the B data when available from C05 and R data from Ivison et al. (2005). In the HDF/GOODS-N field (hereafter simply the GOODS-N field), we use the optical photometry catalogue of Capak et al. (2004), which contains measurements in U , B , V , R , I , and z' . The SMGs in the SSA-13 field have B and R measurements in C05, plus z band measurements from Fomalont et al. (2006) of comparable depth. In the CFRS-14h and SSA-22 fields we use the B and R measurements from C05. For the ELAIS-N2 field, we take our optical data from Ivison et al. (2002), in B , V , and R . The

¹¹ Note that using optical through near-IR SED fitting to obtain both photometric redshifts and stellar mass for SMGs, as done in Dye et al. (2008), is problematic in that both the redshift and mass are sensitive to the choice of spectral template used.

available near-IR data for our sample are more homogeneous, because we obtain all of the near-IR data (I , J , K) from the study of Smail et al. (2004) for all fields with the exception of the GOODS-N field. For SMGs in GOODS-N, we use the I data of Capak et al. (2004), but the J and K data of Smail et al. (2004). We convert all the optical data obtained from the literature to total magnitudes using aperture corrections, generally supplied by the corresponding authors of each data set, to eliminate the effects of differing seeing conditions and photometry aperture size between different data sets.

We note that 4 out of the 67 SMGs from our IRAC-observed sub-sample of C05 SMGs have less than 3 detections across the observed-frame optical–mid-IR wavelength range. While it is difficult to place meaningful constraints on their stellar SED to derive ages and extinction with so many upper limits, we can still place upper limits on their luminosities in a given band, and use mass-to-light ratios derived for other SMGs to place upper limits on their stellar mass. Thus, we retain these galaxies in our sample despite the small number of detections.

3. CALCULATING THE STELLAR MASS OF SMGS

Our approach to determining the stellar masses of SMGs is derived from that of Borys et al. (2005), because, as we discuss below in §3.1, we find that the method typically applied to obtain the stellar mass of intermediate- and high-redshift galaxies (i.e., fitting a stellar population model to each galaxy’s SED to determine its stellar population age, visual extinction, and appropriate mass-to-light ratio) is unable to adequately constrain the stellar mass of individual SMGs in our sample. Rather than assume that the stellar population parameters and masses derived for individual SMGs from SED fitting are correct in an absolute sense, we derive constraints on the stellar population parameters and stellar masses from averages over the SMG sample (§3.2). In doing so, we can only constrain the stellar mass of SMGs in an average sense (the mean and median of the sample). Although we will still present estimates of stellar mass for the individual galaxies for those who wish to use them despite the large uncertainties, we will only discuss the average properties of the sample.

In the discussion that follows, and to obtain the average stellar population parameters of SMGs, we have used version 11.0 of the HYPER-Z photometric redshift software package (Bolzonella et al. 2000) to fit evolutionary population synthesis models to the optical–mid-IR SEDs of the individual galaxies in our sample. HYPER-Z employs χ^2 minimization to derive the best-fit age/time since the start of star formation, optical extinction A_V , and normalization for a given stellar population model. We restricted the code to fit the SEDs at the spectroscopic redshift of each SMG, and required that the best-fit ages be less than the age of the Universe at the redshift of each SMG. We have fitted the population synthesis models of both Bruzual & Charlot (2003, using the Padova 1994 stellar tracks; hereafter BC03) and Maraston (2005, hereafter M05), although in §4 we choose to report results for only one set of models. We utilized the solar metallicity models based on the findings of Swinbank et al. (2004) that SMGs have metallicities consistent with those of UV-selected galaxies of similar redshift, which for the most massive examples have approximately solar metallicities (Erb et al. 2006a), and the findings of Tecza et al. (2004). The BC03 and M05 models are made available with two different initial mass functions (IMFs): the BC03 models have a choice of the Salpeter (1955) IMF or the Chabrier (2003) IMF, while for the M05 models we must choose between the Salpeter (1955) IMF

and the Kroupa (2001) IMF. We preferred to not use the IMF of Salpeter (1955) since observations of local galaxies suggest that this IMF over-predicts the numbers of low-mass stars and thus the mass-to-light ratio (e.g., Blain et al. 1999; Bell & de Jong 2001), casting suspicion on its use in high- z galaxies. Instead, we use the Chabrier (2003) IMF for the BC03 models with a lower mass cutoff of $0.1 M_\odot$ and upper mass cutoff of $100 M_\odot$, and the Kroupa (2001) IMF for the M05 models with the same low-mass cutoff. Although the use of two different IMFs may be somewhat confusing, the two different IMFs predict similar spectral properties and mass-to-light ratios at a given age (BC03), and Tacconi et al. (2008) find that the two IMFs produce similar results to within 15%. To account for dust extinction in our SED fitting, we assumed a simple dust screen model, although it is likely that SMGs contain a variety of clouds of different obscuration attenuating the total observed starlight. We used the Calzetti et al. (2000) extinction law for starburst galaxies, allowing the extinction to vary within a range of $A_V = 0 - 5$ mag. In addition to extinction intrinsic to each galaxy, we also corrected for the modest reddening along the line of sight to each SMG due to the Milky Way using the dust maps of Schlegel et al. (1998). The line-of-sight reddening estimate for each sky field is listed in Table 1.

3.1. Complications In Applying Standard SED Modeling Techniques to Estimate M_* for SMGs

3.1.1. Constraining Star Formation History of SMGs

For our stellar mass study, we had originally intended to allow HYPER-Z to choose the best-fitting star formation history for each SMG from a set comprised of an instantaneous starburst star formation history (which is equivalent to a simple stellar population or SSP), a continuous star formation history, and exponential star formation histories of the form

$$\text{SFR}(t) \propto \exp(-t/\tau), \quad (1)$$

where $\tau = 0.1, 0.25, 0.5, 1, 2$, and 5 Gyr, and thus obtain an unambiguous stellar population age, A_V , and stellar mass-to-light ratio which could be used to calculate the stellar mass of each galaxy. However, careful inspection of our tests utilizing the various star formation histories reveals that for many SMGs in our sample, the fits could not indicate a unique best-fit star formation history. We find that the values of χ^2_ν corresponding to the best fit A_V , age, and SED normalization are extremely similar between even just this restricted set of star formation histories, as are the appearances of the fits. Admittedly, for some SMGs in the sample with relatively few photometric constraints or anomalous observed-frame optical photometry, such a result is not unexpected; however, we encounter the same ambiguity among galaxies with the most complete and accurate photometric data. We illustrate the problem in Figure 1, where we show the observed SED of a typical SMG at $z \sim 2.5$ with excellent photometry, fit by a range of different simple star formation histories, using models of both BC03 and M05. Despite the broad range of photometric data in Figure 1 ($UBVRiz'JK+IRAC$), nearly all of the star formation histories can produce fits of similar likelihood (e.g., 4 of the 6 histories shown produce χ^2_ν values within ± 0.01 of each other for the BC03 models, and all of the χ^2_ν values correspond to a probability of 40–70% of exceeding χ^2 for the number of degrees of freedom), with ages varying from ~ 10 Myr to ~ 2 Gyr and extinction in the range $A_V = 1.5 - 2.4$ mag.

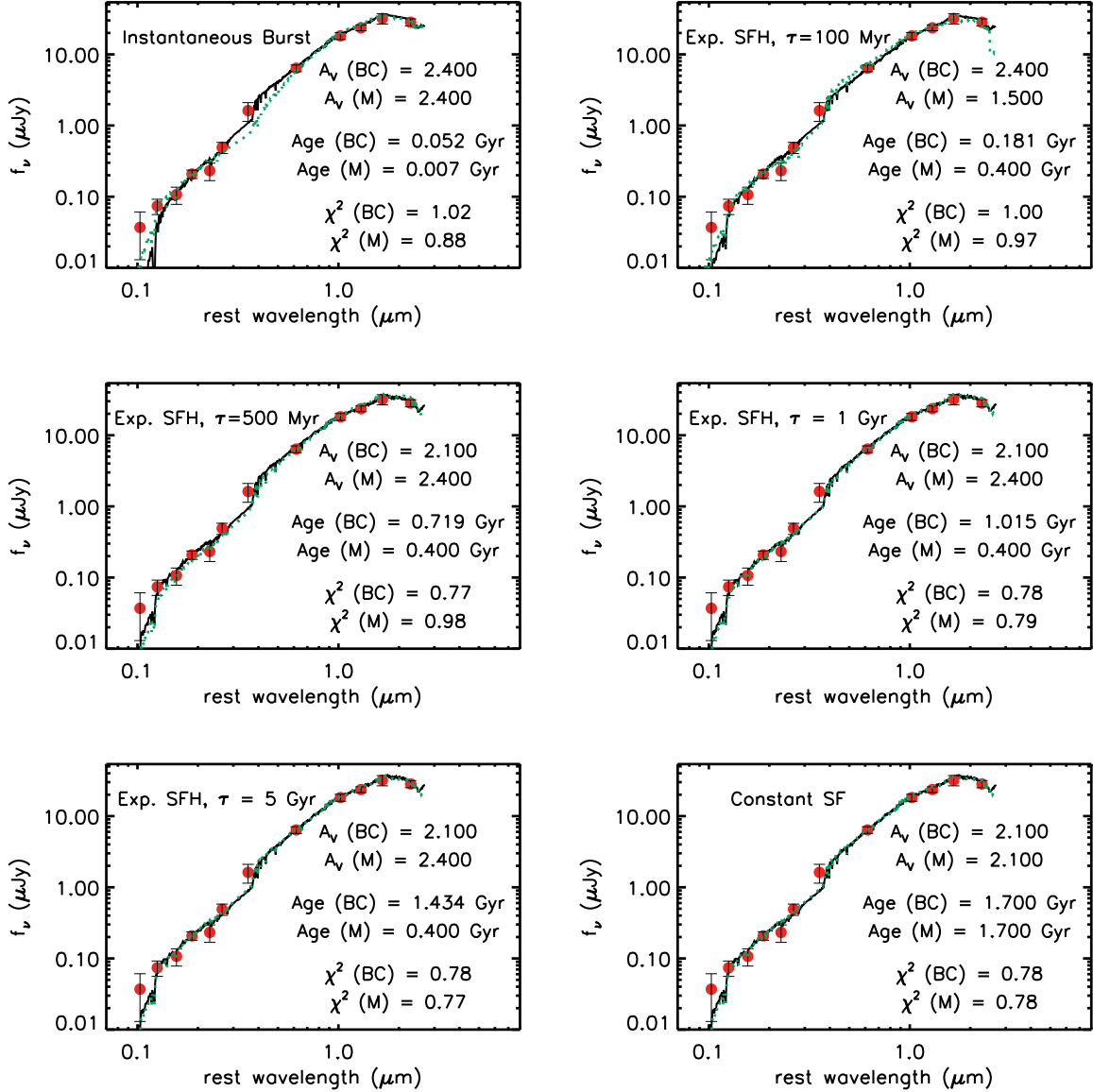


Figure 1. Fits of several different stellar population models of different star formation history to the observed SED of SMM J123707.21+621408.1 (round points) at $z = 2.484$. The best-fit BC03 model spectrum is over-plotted as the solid black line, while the best-fit M05 model is represented by the dotted (green/gray) line. The different fits are nearly equally acceptable in a χ^2 sense. Note that this particular SMG does not display a near-IR continuum excess.

Thus, we conclude that we are unable to place useful constraints on the star formation histories of individual SMGs through fitting such simple stellar population models, as Shapley et al. (2001, 2005), Papovich et al. (2001), and Erb et al. (2006b) also find for UV-selected high-redshift galaxies with similarly broad wavelength coverage. Since the best-fit ages are strongly dependent on the assumed star-formation history (the instantaneous burst models tend to produce the youngest ages, while the continuous star formation models tend to produce the oldest ages, see, e.g., Maraston et al. 2010), we are also unable to effectively constrain the ages of individual galaxies and thus the appropriate mass-to-light ratio of the stellar populations in individual SMGs without other information on the likely star formation histories, introducing extra systematic uncertainties into the stellar mass calculations, on top of any resulting from the stel-

lar models themselves.

Some of our inability to constrain the star formation history and the stellar population ages stems from the available photometric data for SMGs. A small subset of SMGs in our sample (10 out of 67) possess seemingly anomalous observed-frame optical photometric data; for these galaxies, the universally-high χ^2_ν values indicate that none of the stellar population models adequately describe the SED¹². Yet, even when the wavelength coverage and data quality are excellent (e.g., the GOODS-N field), we still may have insufficient information. The determination of age from stellar

¹² The causes of the anomalous photometry are unknown, as no notes are available from the literature data sources for these galaxies. In a few cases, the rest-frame wavelengths of the discrepant data suggest a contribution from an emission line; however, in the remaining cases the optical counterpart could have been mis-identified or the photometric error is larger than stated.

population models relies heavily on the shape of the Balmer break or 4000 Å break in the SED (see, e.g. Kriek et al. 2008; Whitaker et al. 2010)¹³. Unfortunately, for only up to a third of SMGs in our sample do we see a suggestion of a break in the continuum near 4000 Å, and we usually do not have enough photometric data points for our SMGs in the critical area of the Balmer/4000 Å break to clearly delineate the location and the shape of the spectral break. In addition, the well-known degeneracy between age and extinction (e.g., Sawicki & Yee 1998; Shapley et al. 2001), in which a reddened, young starburst population can look similar to an older, unextincted stellar population, is also probably contributing to the ambiguity in the stellar ages. However, we expect that much of the difficulty in constraining stellar population ages is likely to arise from the application of relatively simple stellar models to what is likely an intrinsically complex mix of stellar populations of differing metallicity, reddening, and age. Accordingly, we could make use of stellar population models which employ more complex star formation histories, such as short bursts on top of an exponential star formation history (e.g., Borch et al. 2006; Kaviraj et al. 2007; Dye 2008); however, we feel that doing so is not justified because the observational data are insufficient to constrain even simple star formation histories and cannot provide a unique solution. We also stress that the uncertainties here, for SMGs with known redshifts, are far less than if the redshift also has to be derived from the photometric fit.

The star formation history, and by extension, age, of a stellar population are critical elements in determining the appropriate M/L ratio needed to accurately convert a single galaxy’s stellar luminosity to stellar mass. However, if one is willing to forego accurate masses for individual galaxies, one may take advantage of statistics to obtain reasonably precise average and typical stellar masses from a large sample of individual galaxy masses which are much more uncertain. Fortunately, the light-to-mass (L/M) ratios of stellar populations of different star formation histories at ages above 50 Myr, shown in Figure 2 for a sample of star formation histories, have a narrower range of values than the ages themselves and are thus less uncertain than the ages: for example, in the M05 stellar population models, the L/M ratio of an instantaneous burst (IB hereafter) population with age 100 Myr differs by only 20% from that of a constant star formation (CSF hereafter) population with age 2 Gyr. At any age in the range 50 Myr to 3 Gyr (approximately the age of the universe at $z \sim 2$), the L/M of the star formation history with typically the lowest L/M ratio (IB) differs by only a factor of 2–3 at most from that of the star formation history with the highest typical L/M (CSF). So, with no constraint on the star formation history, we can still constrain the stellar masses of individual galaxies to within a factor of 2–3, neglecting other systematic uncertainties. If we assume the star formation histories of individual SMGs are uniformly distributed over the range of possible histories, which is reasonable because our attempts to fit the SEDs of SMGs with a variety of star formation histories revealed no single preferred history over the entire sample, the average star formation history for the population and the average L/M ratio should exhibit less dispersion than those asso-

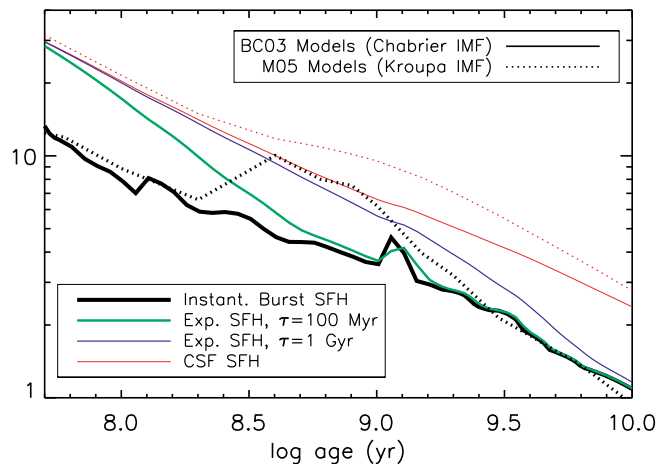


Figure 2. L_H/M_* as a function of time since onset of star formation for solar-metallicity population synthesis models of BC03 and M05. Solid lines represent models of BC03, while dotted lines represent the models of Maraston (2005). The increase in L_H/M_* near $\log \text{age} = 8.5$ in the Maraston (2005) burst model marks the onset of the TP-AGB phase. Because at any age in between 50 Myr and 3 Gyr the L_H/M_* of the star formation history with typically the lowest L_H/M_* ratio (IB) differs from that of the star formation history with the highest typical L_H/M_* (CSF) by at most a factor of 2–3, we can constrain the stellar masses of individual SMGs to within a factor of 2–3 without knowing the star formation history.

ciated with individual galaxies. Consequently, the uncertainty in the sample-averaged stellar mass derived using the average L/M ratio will be much less than the factor of 2–3 uncertainty in the individual masses.

In the absence of any indication of which star formation history is most appropriate, and with the knowledge that (a) the SED fits of the different star formation histories to our SMG sample are correlated; (b) the best-fit ages are likely to not be representative of the true stellar population since the light we receive is strongly modified by reddening; and (c) the L/M ratios implied by the different star formation histories will be similar to within a factor of a few, we elect to compute stellar masses for our sample which are averages over different possible star formation histories, instead of basing our computation on a particular star formation history. We adopt the approach of Borys et al. (2005), in which we assume a single L/M ratio for the entire SMG sample for each of the IB and CSF histories, and average the resulting masses. We choose these two because they are expected to represent the lower and upper extremes of the stellar properties predicted by the different star formation histories; in averaging their results, we hope to reduce the systematic effects of star formation history so that our stellar mass estimates are correct to within a factor of 2. The mean and median of the stellar masses calculated in this way of the full SMG sample will thus be the best-constrained quantity we obtain.

3.1.2. Near-IR Excess in SMGs and Its Removal

In Paper I, we found that numerous galaxies in our SMG sample display evidence of non-stellar emission in their rest-frame $J-H$ and $H-K$ colors (see Figure 6 in Paper I), by comparing to samples of “normal”, non-active local galaxies and local ULIRGs. Upon close examination of the observed SEDs of our sample, we find that approximately 20% of the sample display a clear red upturn in the rest-frame near-IR portion of their SED. The red upturn suggests the presence of hot dust and possibly an obscured AGN, since stellar SEDs typically fall past the $1.6 \mu\text{m}$ stellar peak. An

¹³ Kriek et al. (2008) show, using their sample of $z \sim 2$ massive red galaxies with spectroscopic redshifts, that the best-fit ages obtained through stellar population synthesis modeling of SEDs constructed using broadband JHK photometry have a mean absolute deviation of a factor of ~ 3 relative to the ages derived from SEDs constructed using low-resolution near-IR spectra.

additional 50% of the SMGs in the sample display smaller near-IR excesses redward of the $1.6\,\mu\text{m}$ stellar peak similar to those found in $24\,\mu\text{m}$ -bright luminous IR galaxies and K -band selected galaxies at $0.5 < z < 2.0$ by Magnelli et al. (2008) and Mentuch et al. (2009). These authors suggest that the excess arises from very small, hot dust grains in star formation regions, comparable to the near-IR emission detected from Galactic cirrus (Flagey et al. 2006) and reflection nebulae (e.g., Sellgren et al. 1983) as well as local star-forming galaxies (e.g., Lu et al. 2003), which can be described by graybody emission at temperatures $\sim 1000\,\text{K}$. 56% of our sample also meet the criterion of Alonso-Herrero et al. (2006) for IRAC power-law galaxies (PLGs; power law slope $\alpha > 0.5$), which those authors consider to be obscured AGNs. Yet, it is not completely clear that the PLG classification can generally be attributed to AGN since Donley et al. (2008) find that star forming ULIRG templates at $z > 2.6$ meet the PLG criteria as well (indeed, three of the four SMGs that show no evidence of SED upturn but have $\alpha > 0.5$ are at $z > 2.8$). Regardless of whether or not the origin of the observed excess continuum emission is an obscured AGN or star formation regions, its contribution to the near-IR emission of $\sim 70\%$ of the SMGs in our sample must be removed in order to derive the most representative stellar luminosity and mass.

We remove the non-stellar continuum contributions to the near-IR emission of our SMG sample by assuming that the total observed SED can be represented as a sum of a stellar population model and a power law (PL) of the form $f_\nu \propto \nu^{-\alpha}$ representing the excess, where f_ν is the flux density at frequency ν . Note that, if the excess is in fact due to graybody dust emission in star forming regions rather than dust heated by an obscured AGN, the PL model will still be approximately correct, since the modified Planck function describing a graybody can be approximated as a PL over a small range of wavelength (e.g., a graybody of temperature $700\text{--}1000\,\text{K}$ and emissivity $\epsilon_\nu \propto \nu^1$, appropriate for small dust grains in star-forming regions, can be approximated by a PL with index ranging from -1.8 to -4 in the wavelength range $2\text{--}3\,\mu\text{m}$, depending on the temperature). However, if the excess is due to a $3.3\,\mu\text{m}$ polycyclic aromatic hydrocarbon (PAH) emission line, the PL model will not improve the fits. We scale the PL to the IRAC $8.0\,\mu\text{m}$ data point, and denote this scaled PL as the maximum possible PL contribution. We then subtract from *all* the observed photometry increasing fractions of the flux in this scaled PL, in steps of $0.1 \times$ (maximum PL contribution) and fit the BC03 and M05 stellar population models to the PL-subtracted data points. The PL fraction which results in the lowest value of χ_ν^2 gives us the luminosity of stars only, which we can then use to find the stellar mass. We estimate the error in the PL fraction by determining the PL fractions which result in a change of $\Delta\chi_\nu^2 = 1$ above and below the best-fit PL fraction.

The choice of the best PL index to use in our PL removal is not obvious, because differing obscuration levels can cause the rest-frame near-IR PL slope of hot dust emission to vary between galaxies even when the AGN powers the dust emission (e.g., Simpson & Rawlings 2000). Observationally-derived near-IR PL slopes for local unobscured, type-1 AGN have a typical value of $\alpha \sim 1\text{--}1.5$ (e.g., Malkan & Filippenko 1983; Edelson & Malkan 1986; Neugebauer et al. 1987), whereas the range for local Seyfert 2 nuclei is $\alpha \sim 2\text{--}4$ (e.g., Alonso-Herrero et al. 2003). Obscured starbursts will have similar near- and mid-IR PL slopes

to obscured (type 2) AGN: as mentioned in the previous paragraph, graybody dust emission from star forming regions can be approximated over $\lambda \sim 2\text{--}3\,\mu\text{m}$ as a PL with $\alpha \sim 2\text{--}4$. We initially chose to use a PL index of $\alpha = 2$, based on the observed average mid-IR continuum slope for SMGs with IRS spectra, $\alpha_{\text{MIR}} = 1.97 \pm 0.22$ (Menéndez-Delmestre et al. 2009). However, for some galaxies in our sample, the ν^{-2} PL is too shallow and results in a very poor fit; thus, we have allowed the PL in our continuum removal to have the form ν^{-2} or ν^{-3} , whichever best fits the data in a χ^2 sense for each SMG. By allowing 2 different possible values of the PL index, we introduce an additional uncertainty into our stellar masses; however, the uncertainty in the average mass is small (see §3.3). The results of our SED fits suggest that $\alpha = 3$ typically produces a better fit to the observed data overall: for the 82% (72%) of the SMG sample which have a non-zero best-fit PL contribution at observed-frame $8.0\,\mu\text{m}$ using the M05 IB (CSF) models, 70% (79%) have best-fit PL indices of $\alpha = 3$ while 30% (21%) have best-fit PL indices of $\alpha = 2$. When the BC03 stellar models are used in the SED fits, the relative fractions change somewhat: for the 70% (79%) of the sample with a non-zero best-fit PL fraction for the IB (CSF) star formation history, 74% (81%) have best-fit PL indices of $\alpha = 3$ while 26% (19%) have best-fit PL indices of $\alpha = 2$.

We note that when we extrapolate the observed-frame $24\,\mu\text{m}$ flux from the $8.0\,\mu\text{m}$ flux based on the best-fit PL fraction, the extrapolated value exceeds the observed $24\,\mu\text{m}$ flux in $\sim 50\%$ of cases when $\alpha = 3$ (the median over-prediction for that 50% of the sample is a factor of 2.3) and for $\sim 20\%$ of the sample when $\alpha = 2$ (by a median factor of 1.5). The $\sim 50\%$ and $\sim 80\%$ which are not over-predicted by $\alpha = 3$ and $\alpha = 2$ PLs, respectively, are under-predicted. The over-prediction of the rest-frame mid-IR flux based on the rest-frame near-IR PL implies that the near-IR and the mid-IR require different PL slopes. This phenomenon is observed in local Seyfert galaxies (e.g., Edelson et al. 1987; Alonso-Herrero et al. 2003), and can occur when an unobscured nucleus' emission is modified by a foreground reddening screen (e.g., its host galaxy). Such curvature in the mid-IR SED of high- z QSOs is also found by Gallagher et al. (2007), who find that the rest-frame $8.0\,\mu\text{m}$ luminosities of their sample are over-predicted by factors ranging from 1.25–2.5 upon extrapolating the best-fit observed-frame $1.8\text{--}8.0\,\mu\text{m}$ PL to rest-frame $8.0\,\mu\text{m}$. Thus, our choice of near-IR PL indices for fitting are not necessarily invalidated by over-predicting the observed $24\,\mu\text{m}$ flux.

An alternate approach to fitting the near-IR excess emission in the observed SED for the purpose of estimating stellar masses is to fit a combination of stellar population synthesis models and AGN (type 1 and/or 2) templates from the literature (see, e.g., Merloni et al. 2010). However, we prefer the stellar population plus PL approach over the use of templates for several important reasons. First, because we have no spatial information for the near-IR excess observed in our SMGs, and because SMGs are strongly star-forming galaxies, we are hesitant to assume a priori that the excess arises from an AGN when dust heated by star formation could also explain the observations. The vast majority of our SMG sample are adequately fit in the rest-frame UV and optical by stellar models only, so it is not unreasonable to consider the case in which stellar radiation powers the near-IR excess. Setting aside our wish to not make assumptions regarding the origin of the near-IR excess, our observation that the SMG SEDs can generally be described by stellar emission argues against

a need for type-1 AGN templates; a case could still be made, though, for the use of type-2 AGN templates. On the other hand, our stellar population model plus PL representation is a good reproduction of a type-2 AGN SED, since a type-2 AGN SED is dominated by stellar light in the rest-frame optical and PL continuum in the near-IR. Moreover, by using our stellar model plus PL approach it is actually more straightforward to separate the contributions of stellar emission and featureless continuum to an SED than would be possible using a stellar model and a type-2 AGN template, because the type-2 AGN template may contain some contribution from the AGN host galaxy in the near-IR. Finally, and most importantly, we prefer to use our PL removal model rather than AGN templates because the PL model permits some flexibility in the near-IR PL index. We discussed above how our efforts to determine the most appropriate near-IR PL index for the removal of the continuum excess revealed that we could not fit all of the SMGs in our sample with a single PL index; PL index variation in the near-IR is also observed in local AGN. Yet, by using an AGN template to fit the observed SEDs, we would have only one option for the near-IR PL index, which may or may not be appropriate for our sample. For example, the average optically-bright (type-1) QSO SED constructed from Sloan Digital Sky Survey QSOs by Richards et al. (2006), frequently used as an AGN template, has a PL index $\alpha = 1.8$ in the wavelength range $1\text{--}3\text{ }\mu\text{m}$. This PL index will somewhat under-subtract the near-IR continuum component in those SMGs which are best fit by $\alpha = 2$ and significantly under-subtract the continuum for the SMGs which are best-fit by $\alpha = 3$ (the majority of the sample). The composite type-2 AGN SED of Polletta et al. (2007), another commonly-used AGN template, has a near-IR PL index $\alpha = 1.3$ between 1 and $3\text{ }\mu\text{m}$; this template will thus significantly under-subtract the continuum component in nearly our entire SMG sample.

We illustrate the effects of our PL removal procedure on a typical SMG in our sample showing a near-IR upturn in Figure 3. We first show the observed optical–IRAC photometry and the best-fit CSF stellar population model from M05 to the observed data; the χ^2_ν of the fit indicates that the fit is poor. We then show the best-fit combination of ν^{-2} PL and CSF stellar population model to the same observed photometry as well as the flux contributed by the PL component. Finally, we show only the stellar component of the fit from the middle panel which allows us to determine the stellar luminosity of the SMG: the PL-subtracted photometry is plotted along with its corresponding best-fit CSF model. Note the significant improvement in the χ^2_ν statistic of the stellar model fit when the PL component is subtracted as well as the more appropriate age of the best-fit model. For $\sim 60\%$ of the SMGs the best χ^2_ν value of the fit improves when we subtract a PL contribution from the observed SED; indeed, for $\sim 20\%$ of the sample, the best χ^2_ν of the fit decreases by a factor of 2 or more when we subtract the PL contribution. In Figure 4 we show the results of the best CSF stellar population plus PL fit to the observed photometry for the SMGs in our sample requiring PL contributions at observed-frame $8.0\text{ }\mu\text{m}$ greater than 70% , for which the fits improved the most with the inclusion of the PL component. In Figure 6 we show the best CSF stellar model plus PL fits for the remainder of the SMGs, for which the necessity of a PL SED component can be more ambiguous. We note that, for both Figures 4 and 6, the IB fits are visually similar to the CSF fits, although the best-fit PL contributions differ between the IB and CSF star formation histories for $\sim 60\%$ of

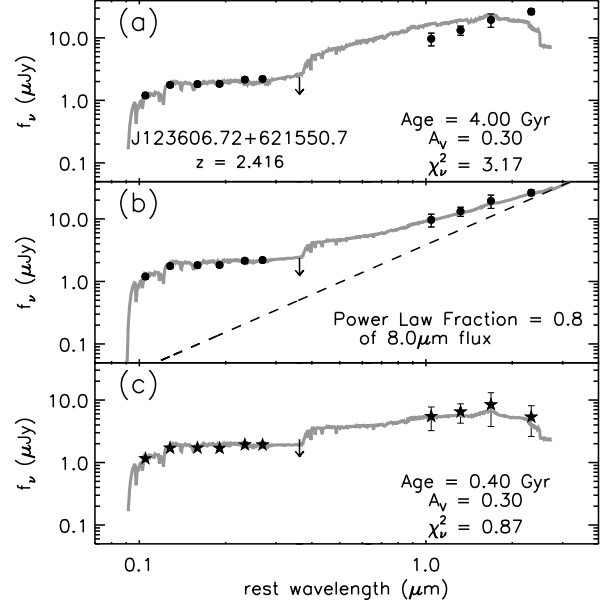


Figure 3. Example of stellar population model plus power-law fraction SED fitting used for our sample of SMGs. Panel (a): The observed *UBVRIZ'JK*–IRAC photometry (round points) for a typical SMG with a near-IR excess is shown with the best-fit CSF stellar population model of M05 to that data. The near-IR excess is most clearly seen at $\lambda_{\text{rest}} > 2\text{ }\mu\text{m}$. We note that the requirement that the age of the best-fit model be physical was relaxed in this particular case to allow the fit to converge. Panel (b): The observed photometry for the same SMG is shown along with the best-fit combination of ν^{-2} power law and CSF stellar population model from M05. Panel (c): The power-law subtracted photometry (black stars), representing the total stellar contribution to the observed SED is shown with the best-fit CSF stellar population model from M05 to those data points only. Note from panel (a) that the unphysical age of the best-fit stellar population model (it is greater than the age of the universe at $z = 2.4$) and the statistically poor fit are indications that the stellar population model alone is insufficient to account for the near-IR emission from this SMG.

our sample for both the BC03 and M05 models. In contrast to the similar visual appearance of the IB and CSF fits, the best χ^2_ν values for the IB star formation history are 10% greater (BC03 models) and 16% greater (M05 models), on average, than the best χ^2_ν values for the CSF star formation history.

3.2. Stellar Mass Calculation Details

We calculate a stellar mass (M_*) for each SMG from the de-reddened, best-fit-power-law-subtracted absolute H magnitude (M_H). K -band light has been used to determine the stellar mass in past studies of the stellar mass of SMGs (e.g., Borys et al. 2005; Michałowski et al. 2010) because of its low sensitivity to previous star formation history and dust obscuration. We instead choose to use the rest-frame H band to estimate M_* for our sample of SMGs to benefit from the low extinction of the near-IR bands while minimizing the uncertain influence of thermally pulsating asymptotic giant branch (TP-AGB) stars on the model K -band light-to-mass (L/M) ratio in the M05 stellar population models. The change in H -band L/M ratio induced by the appearance of a dominant solar-metallicity TP-AGB population at ages of $\sim 0.5\text{--}1.5\text{ Gyr}$ is a factor of ~ 2 , smaller than the change in the K -band ratio. Calculating the mass from M_H also has the advantage that the contribution of the power-law emission is naturally lower in the H -band than in K -band, so the uncertainty introduced due to our subtraction of the power-law component is smaller. A final reason for the use of H -band in deriving the stellar masses is that for the highest-redshift ($z > 3$) SMGs in our

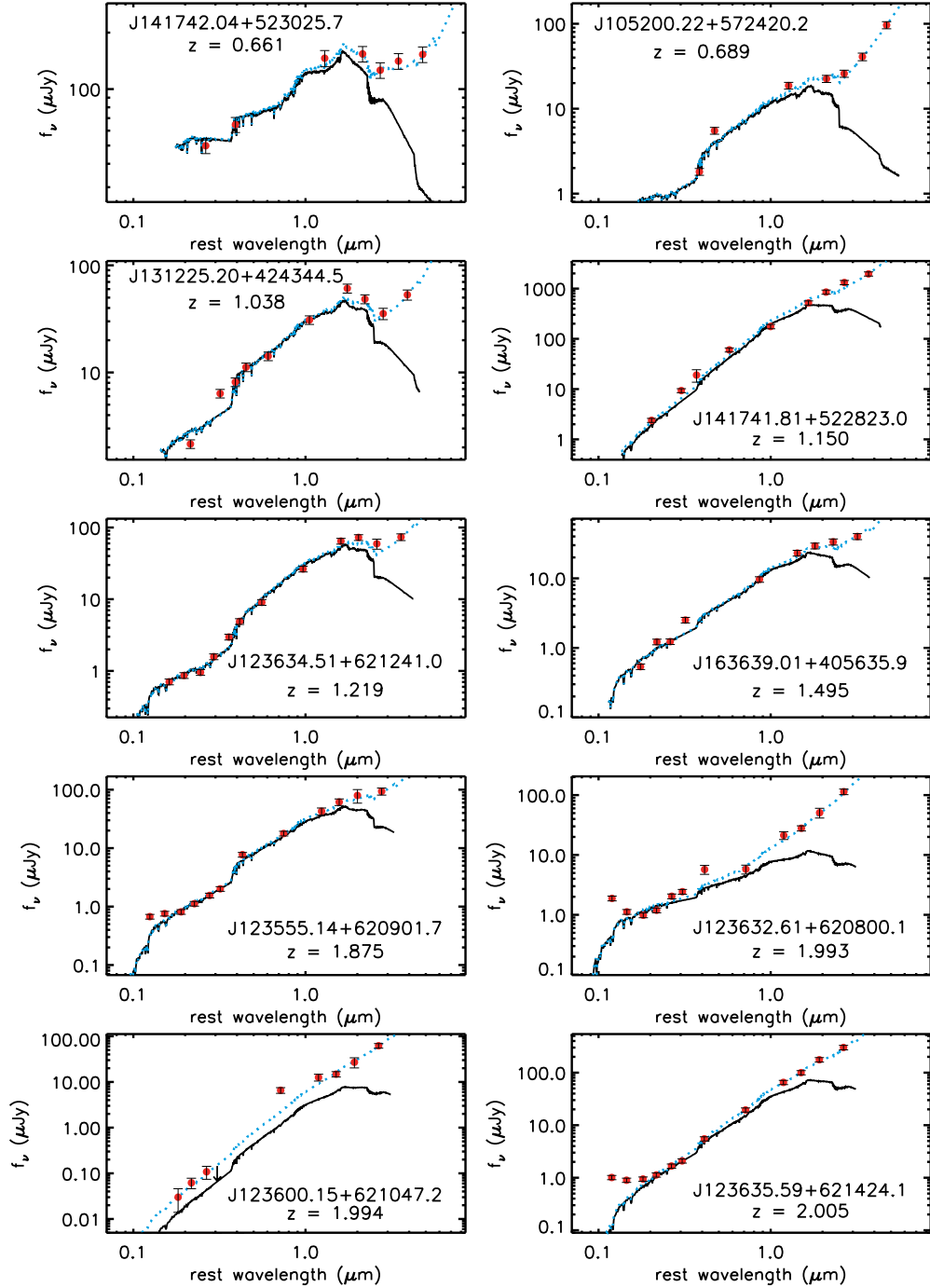


Figure 4. Rest-frame UV through near-IR SEDs of spectroscopically-identified SMGs in our sample unambiguously requiring significant near-IR power law components to fit the observed SED. Round points are observed photometric data, while non-detections are indicated by downward arrows originating from the measured upper limit. The best-fit CSF model of M05 is over-plotted as the black line. The best-fit combined stellar population model plus best-fit power law is represented by the dotted (blue/gray) line. The UV excess displayed by several of these SMGs cannot be reproduced by stellar or near-IR power-law components or a combination of the two.

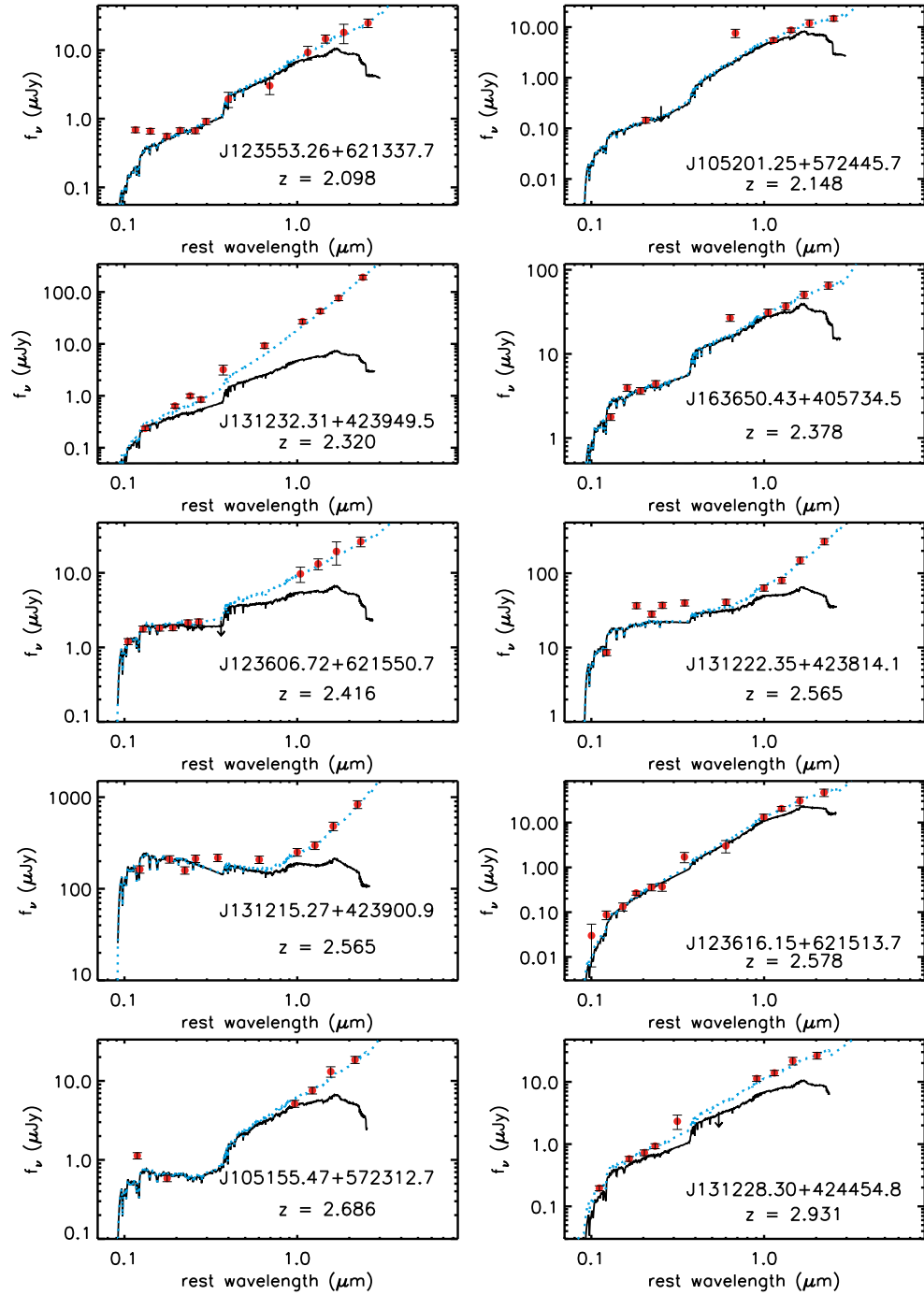


Figure 5. Figure 4 continued.

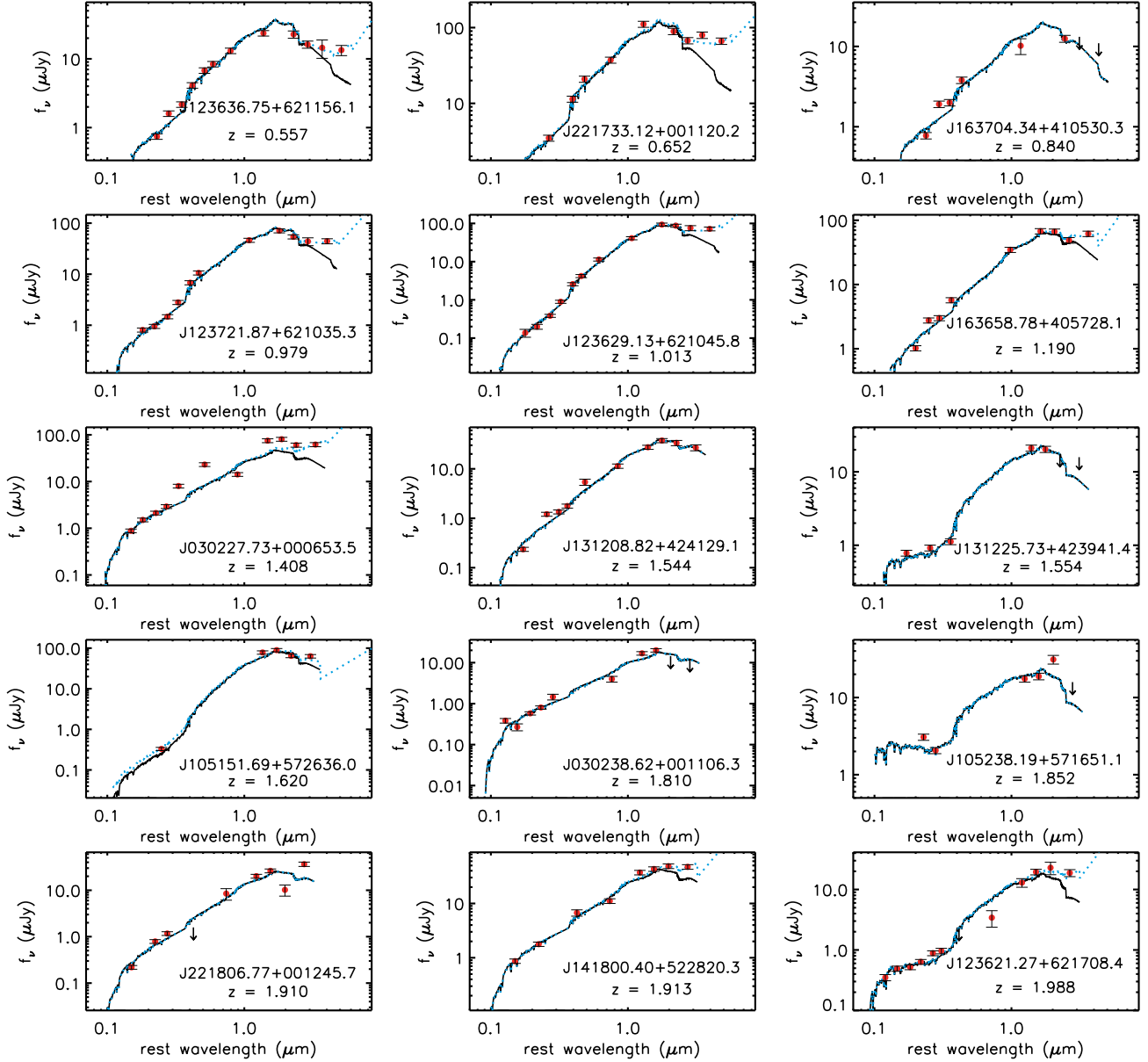


Figure 6. Rest-frame UV through near-IR SEDs of remaining SMGs in our sample. Symbols and lines are as in Figure 4. The large variation in non-stellar near-IR continuum contribution within the sample is apparent when comparing to Figure 4, ranging from pure stellar emission to nearly pure power-law emission.

sample, the longest-wavelength IRAC observations ($8.0\,\mu\text{m}$) do not quite sample rest-frame K , so calculations of the absolute K magnitude (M_K) for these sources are not constrained by the available data without extrapolation.

In §3.1.1, we explained our rationale for adopting the stellar mass calculation method of Borys et al. (2005), which uses a single L/M ratio for the entire sample of SMGs for a given star formation history. We obtain this L_H/M_* ratio for each star formation history (IB and CSF) by finding the average of the best-fit model ages over the SMG sample for the fits of that star formation history and taking the L/M ratio for that star formation history corresponding to that average age. Thus, for the BC03 models we use $L_H/M_* = 5.8 L_\odot M_\odot^{-1}$ for the CSF history and $L_H/M_* = 7.9 L_\odot M_\odot^{-1}$ for the IB history, corresponding to average sample ages of 1.5 Gyr and 140 Myr, respectively. From the M05 stellar models we derive an average

age and L/M ratio of 1.6 Gyr and $L_H/M_* = 7.9 L_\odot M_\odot^{-1}$ for the CSF history, and 120 Myr and $L_H/M_* = 8.5 L_\odot M_\odot^{-1}$ for the IB history.

We calculate the stellar mass for each SMG for each of the CSF and IB star formation histories using the L_H/M_* ratio for that history and M_H from the normalization of the SED fit of that star formation history, then average the masses obtained from the IB and CSF histories to obtain our final stellar mass estimate for each SMG. We estimate the uncertainty in the stellar masses by dividing in half the difference in the masses resulting from the CSF and IB star formation histories, since these values tend to represent the maximum and minimum values of the L_H/M_* ratio among the various simple star formation histories we examined (see Figure 2). We thus attempt to represent the systematic effects of star formation history and L_H/M_* ratio in our uncertainty estimates, which are much more significant than the random errors in the model fitting

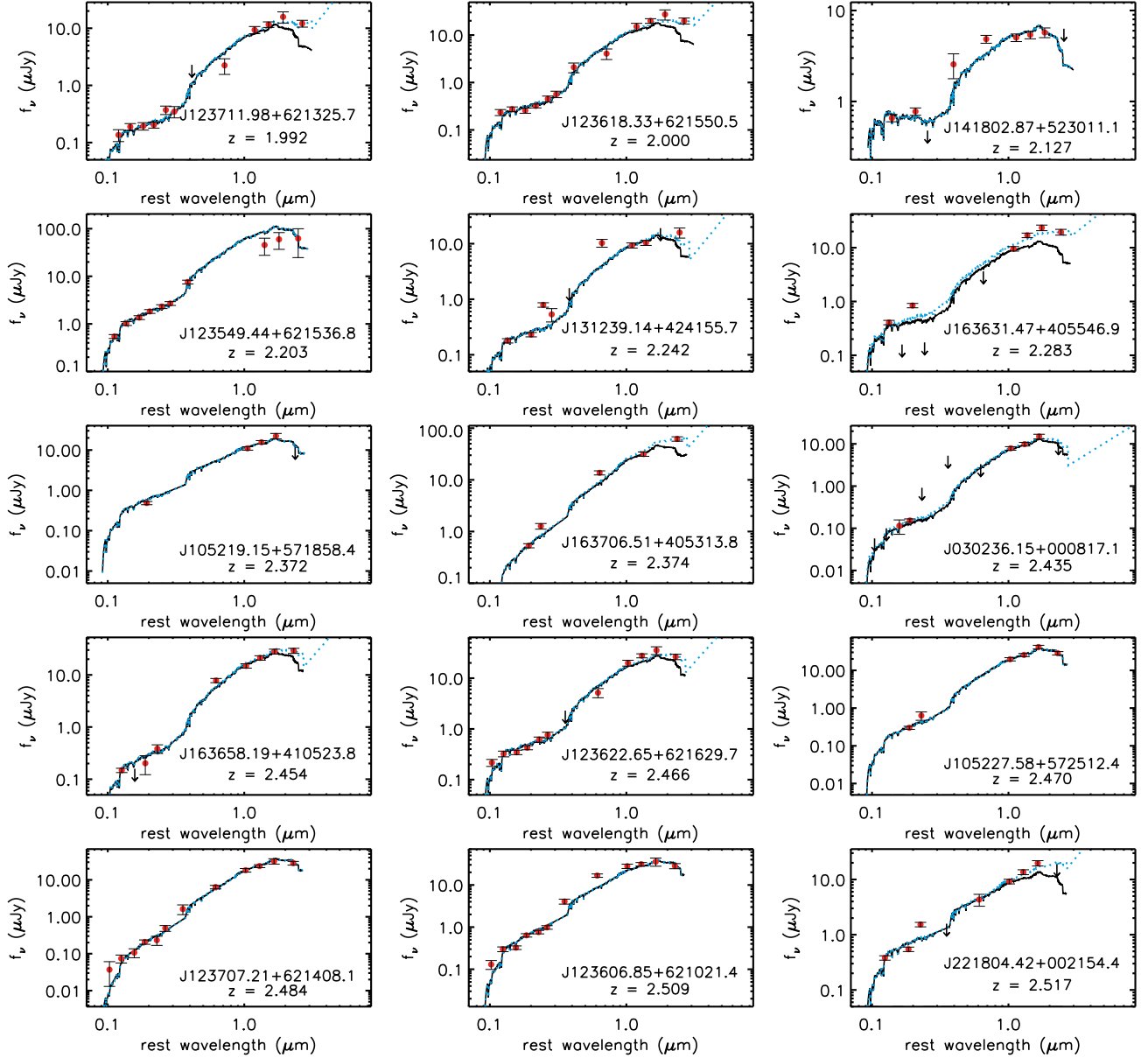


Figure 7. Figure 6 continued.

due to the photometric uncertainties (see, e.g., Muzzin et al. 2009). However, we caution that myriad systematic errors are still possible for our mass estimates based on the assumptions we have made, as we discuss in the next section.

3.3. Sources of Systematic Uncertainty in Median M_*

Although the median stellar mass of our SMG sample is the best-constrained quantity we derive in our study, the median stellar mass still has associated random and systematic uncertainties which can be significant and must be mentioned. We have estimated the random error in our median stellar mass by randomly perturbing the observed photometry of our sample within its associated error bars and carrying out our SED fitting and mass estimation procedure on the perturbed data for the galaxies. By analyzing the statistics over many trials (where each trial produces a median stellar mass for the sample), we find that the standard deviation of the median

stellar mass, which we call the random error in the median of our sample, is 11%. Because the random error associated with our SED fitting is only $\sim 10\%$, the overall uncertainty in our median stellar mass is dominated by systematic uncertainty. On the whole, we expect the dominant systematic uncertainty arises from our use of stellar population synthesis models to obtain a L/M ratio; as this uncertainty is difficult to quantify and affects nearly all studies of the stellar mass in high-redshift galaxies similarly, we refrain from discussing it at length. Rather, we restrict ourselves to a brief summary of the more concrete systematic effects and their impact on our median stellar mass, noting that many of the sources of uncertainty have been explored in detail elsewhere (e.g., Papovich et al. 2001; van der Wel et al. 2006; Conroy et al. 2009; Muzzin et al. 2009). We further note that, in principle, systematic errors in the stellar mass calculations could occur within our sample between the different sky fields

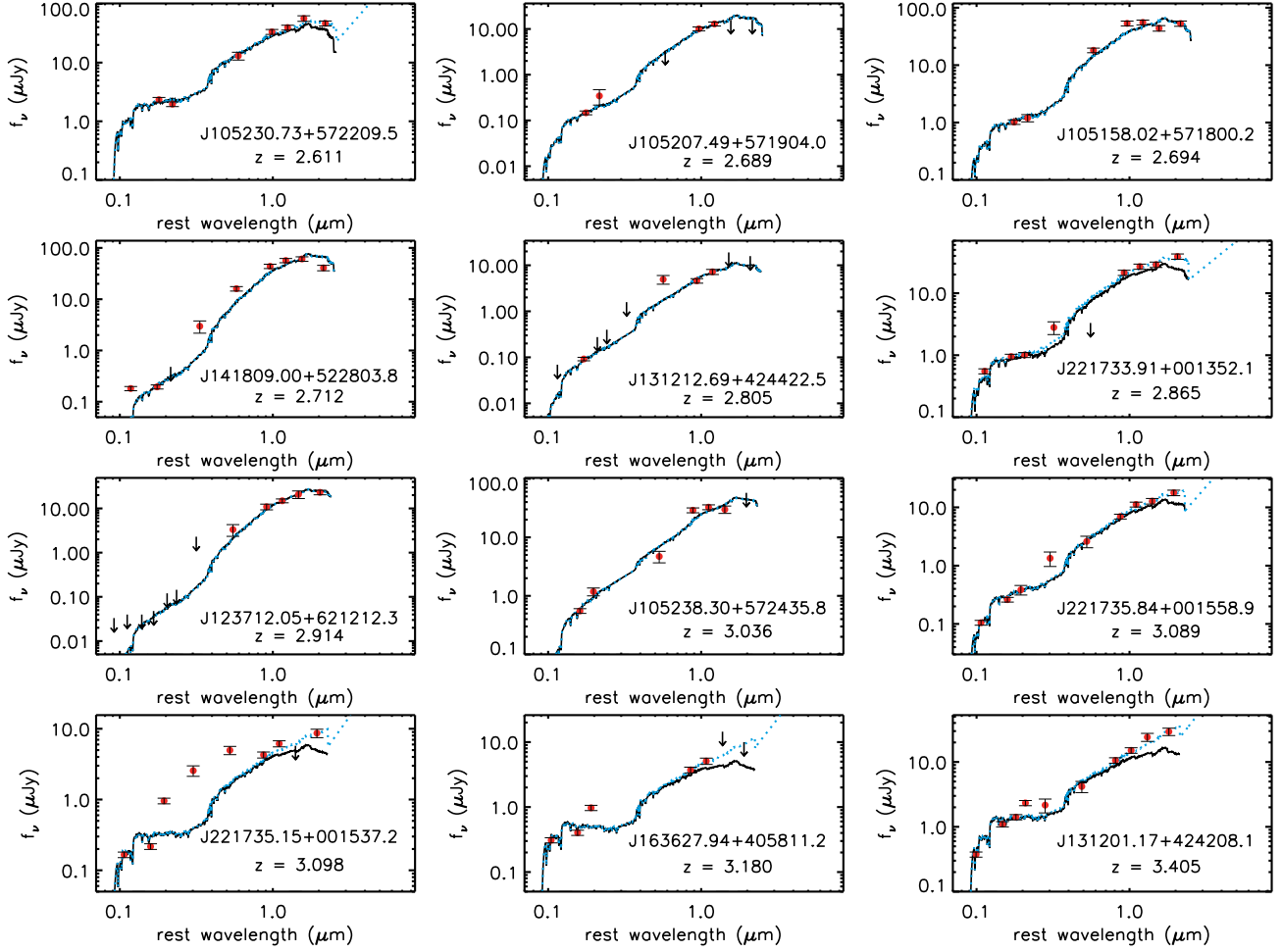


Figure 8. Figure 6 continued.

because some of the fields have fewer optical photometric data points to constrain the SED models from which derive the ages and M/L ratios. However, in practice, since our aim is to constrain the average stellar mass over the SMG sample and not individual galaxy masses, this particular source of systematic error is not significant: tests varying the number of optical photometric data points used in fitting the GOODS-N subsample of SMGs (which has the most photometric data of all the fields in our sample) reveal variation of no more than 0.1 dex in the mean and median stellar mass.

Relatively minor contributions (~ 10 – 20% individually) to the systematic uncertainty in our median stellar mass arise from our metallicity and extinction law assumptions and our removal of the near-IR continuum excess in fitting the SEDs of our sample of SMGs. As shown by Muzzin et al. (2009) and Conroy et al. (2009), the assumption of a single metallicity in our fitting introduces uncertainties in the stellar masses of 10–20%. We have estimated the uncertainty in the median stellar mass resulting from use of the Calzetti et al. (2000) extinction law for starbursts to be also 10–20% by fitting stellar population models to the SEDs of our sample assuming the extinction laws for the Milky Way (Fitzpatrick 1986) and the Small Magellanic Cloud (Prévot et al. 1984; Bouchet et al. 1985). We note that our simplistic treatment of the extinction within SMGs as a uniform dust screen also affects our stellar mass estimates in a way which is difficult to quantify;

yet, as there are essentially no constraints on the distribution of dust and star formation within SMGs, it is difficult to justify the use of more complex extinction models, such as age-dependent extinction (e.g., Poggianti & Wu 2000). The systematic uncertainty in our average stellar mass estimate associated with our near-IR continuum removal procedure arises from the index of the PL subtracted from the observed SED to obtain the stellar H -band luminosity. We have estimated this uncertainty as 10–15% by comparing the stellar masses of the individual galaxies in our SMG sample resulting from the assumption of PL indices $\alpha = 2$ and $\alpha = 3$.

The systematic uncertainty in our typical stellar mass estimate from our choice of IMF is considerably larger than those associated with metallicity, extinction, and choice of PL index. The choice of a particular function effectively introduces a scaling factor into the mass estimates: for example, if we instead chose to use the Salpeter IMF with the BC03 and M05 stellar population models rather than the Chabrier (2003) and Kroupa (2001) IMFs, the median stellar mass would be higher by a factor of 1.6 (Kroupa) and 1.8 (Chabrier). If we assume the systematic uncertainties arising from the choice of IMF, metallicity, extinction law, and PL subtraction are all independent (which may not be correct) and add them in quadrature, we obtain a conservative estimate of the systematic uncertainty in our typical stellar mass of a factor of 1.6–1.8, which is clearly dominated by the IMF systematic. Including the un-

certainty due to the stellar population models will obviously increase the overall systematic error estimate.

We caution that a final source of systematic uncertainty which is not easy to quantify with currently existing observational data may significantly affect our stellar mass estimates. Should a large fraction of the stellar content of SMGs lie within or behind the heavily obscured star formation regions, we are unable to trace its mass since we do not receive its light. In principle, dynamical mass estimates can help assess the amount of mass missing from our estimates, but the currently available dynamical masses for SMGs come from CO or H α observations which may not trace the bulk of the stellar mass. In the future, when precise dynamical masses for our sample are obtained from rest-frame near-IR (i.e., stellar) light, we will be able to fully address this issue. Until then, our stellar masses cannot include this unknowable, but potentially significant, fraction of the stellar mass in SMGs. How much mass is missing from our estimate of the median will depend on how the dust is distributed throughout SMGs, which we discuss further in the next section.

4. RESULTS

In Table 2, we provide for our sample of 65 spectroscopically-identified SMGs the de-reddened values of M_H and the M_* calculated as described in §3.2, as well as averaged V -band extinctions and the $8.0\mu\text{m}$ PL fraction resulting from our stellar population synthesis model plus PL fitting for the M05 stellar models. The results for the BC03 models are largely similar, though with a scaling factor in the stellar masses, so we have chosen not to tabulate those results here. As a brief summary of the differences between the BC03 and M05 results, we find that the absolute H -band magnitudes resulting from the use of the BC03 models are 0.03 mag fainter, on average, than those resulting from the M05 models; the V -band extinctions are equal, on average, between the BC03 and M05 models for the IB star formation history but the extinctions for the CSF star formation history are 0.4 mag higher systematically in the BC03 results; finally, the stellar masses resulting from the BC03 models are systematically 25% higher than those obtained with the M05 models, although we note that a Chabrier IMF has been used for the BC03 results while a Kroupa IMF has been used for the M05 results. We discuss the results contained in Table 2, some of their implications, and some caveats in the sections below, providing the quantities derived from the BC03 models only when significantly different. For our discussion we separate the $z < 1.5$ SMGs from the higher- z galaxies because our focus in this paper is on the high-redshift SMGs which dominate our sample, cover a smaller epoch of cosmic time, and are more important in a cosmological sense in that they contribute more significantly to the cosmic star formation rate density ($z \sim 2$ SMGs with $S_{850} > 4\text{ mJy}$ contribute $\sim 25\%$ of the overall star formation rate density at that redshift, while similarly bright $z \lesssim 1$ SMGs contribute $\sim 10\%$; C05; Wardlow et al. 2011). Moreover, the low- z SMGs are known to differ somewhat from the high- z SMGs in that they are typically less far-IR-luminous (C05), and thus may have different characteristics from the high- z sub-sample overall.

4.1. Contribution of Non-Stellar Near-IR Emission in SMGs

Through fitting the combination of stellar population models and a PL to the observed SED of our sample of SMGs, we have placed constraints on the fraction of the observed-frame

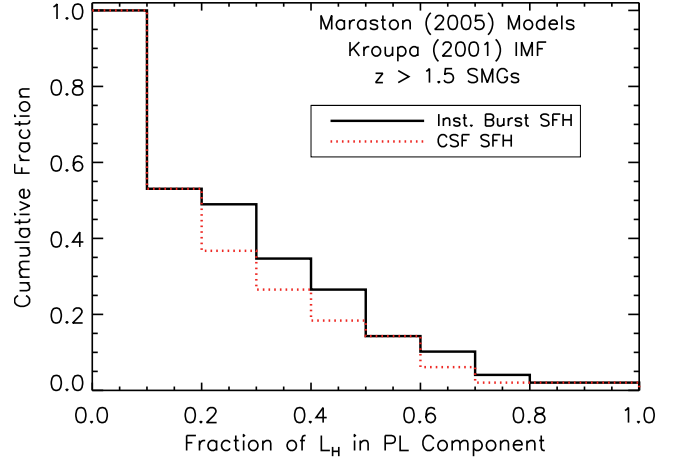


Figure 9. Cumulative distribution of the fraction of rest-frame H -band luminosity in the power-law component for $z > 1.5$ SMGs, based on the best-fit power law fraction at observed-frame $8.0\mu\text{m}$, using the M05 stellar population models. Approximately half the SMG sample has less than 10% contribution to the rest-frame H luminosity from the power-law component, and 11% of the sample has more than 50% of the H -band emission originating from the power-law component.

$8.0\mu\text{m}$ emission of each SMG which is contributed by a PL component, which we tabulate in Table 2. To make our results easier to interpret, we have converted this best-fit PL fraction at observed-frame $8.0\mu\text{m}$ into the fraction of the total rest-frame H -band luminosity (L_H ; approximately the location of the peak of the stellar emission) of each SMG in our sample contributed by its PL component. In Figure 9 we show the cumulative distribution of the calculated fraction of rest-frame H luminosity in the PL component for the $z > 1.5$ portion of our sample for both the IB and CSF star formation histories using the M05 stellar population models. The distributions of inferred PL fraction are quite similar for the different star formation histories; for each, approximately half of our $z > 1.5$ sample have essentially negligible contributions to their total L_H from a PL component. Of our entire spectroscopic SMG sample, 69% (79%) of the galaxies have non-zero fractions of L_H for the CSF (IB) star formation history; yet for only 11% (for both star formation histories) is the fraction of L_H in the PL component greater than 0.5. For reference, and warning, we list in Table 3 those SMGs for which the fraction of L_H in the PL component is greater than 0.5. Clearly, the majority of our SMG sample are stellar-dominated in rest-frame H , although for much of the sample the stellar mass will be somewhat overestimated (by a median value of 10%, and a mean value of 25%) if we assume that all of the near-IR light is stellar. While the amount by which the stellar masses are overestimated lies well within the errors of our present study (see §3.3), future studies which aim to determine M_* more precisely for individual SMGs will need to remove the non-stellar contribution to the near-IR light.

Interestingly, one of the near-IR PL-dominated SMGs listed in Table 3 also displays a rest-frame UV excess. At least three additional galaxies in our sample also appear to have a UV excess, which are noted in Table 2; we note that because the detection of a UV excess requires a reported observation in the observed-frame U band, which most of sample lack, we are prevented from accurately determining the frequency with which UV excesses occur in our sample. Each of the four UV-excess SMGs

have significant PL contributions in the near-IR, even though three of the four galaxies do not qualify as PL-dominated. For two of these SMGs (SMMJ123632.61+620800.1 and SMMJ123635.59+621424.1) AGN spectral identifications in the observed-frame optical (C05) and X-ray (Alexander et al. 2005) suggest that a type-1 AGN could be the origin of the UV excess; high-resolution imaging of these galaxies in the observed-frame U -band showing a compact morphology would lend additional support to such a hypothesis. However, the other two UV-excess SMGs (SMMJ123553.26+621337.7 and SMMJ123555.14+620901.7) have no AGN signatures in their observed-frame optical spectra, so attributing the UV excess to a type-1 AGN is problematic. For these SMGs, a possible explanation for the UV excess is that a simple uniform dust screen is simply an inappropriate model of the stellar extinction across the entire galaxy, as Poggianti et al. (2001) show for luminous IR galaxies displaying e(a) spectra. For example, in these particular SMGs some portion of the total star formation may be relatively unobscured and contribute some UV flux to the SED, while the dominant star formation activity is heavily obscured. Another possibility is that the UV excess is a result of scattering of obscured AGN light, similar to the origin of the far-UV flux in the local Seyfert 2 galaxy NGC 1068 (e.g., Code et al. 1993; Grimes et al. 1999). High-resolution U -band imaging of these SMGs will also be important to determine the origin of the UV excess.

4.2. Near-IR Stellar Luminosity of SMGs

As a result of our separation of the PL component from the stellar component in the observed SEDs of our sample of SMGs, we have obtained more representative estimates of the rest-frame near-IR stellar luminosity for SMGs. The absolute H magnitudes resulting from our SED fitting procedure are much less dependent on star formation history than the stellar masses, as the absolute magnitudes are calculated from the photometric data point nearest the rest-frame H band by applying a (small) K -correction interpolated from the best-fit stellar population model. Thus, the absolute magnitudes of individual SMGs listed in Table 2 are much better constrained than the stellar masses listed for individual galaxies. Since we fitted both IB and CSF star formation histories to the observed SMG SEDs, we obtain multiple estimates of M_H ; to obtain a single M_H for each SMG for our present discussion and for Table 2, we average the M_H values resulting from the fits of the IB and CSF star formation histories. We estimate the uncertainty as half of the difference between the IB and CSF values; by doing so we take into account the uncertainty in the K -correction determined from the SED models of different star formation history, although we anticipate it is small.

The median of the stellar absolute H magnitude determined in this way for the $z > 1.5$ SMGs in our sample, including the upper limits for galaxies which had fewer than 3 detections in their SEDs, is $\langle M_H \rangle = -25.7 \pm 0.2$ with standard deviation $\sigma_{M_H} = 1.1$ for the M05 models; we note that the median M_H found using the BC03 models is only 0.02 mag fainter. When de-reddened by the median value of A_V , the median absolute H -band magnitude for becomes $\langle M_H \rangle = -26.0$. For the $z < 1.5$ SMGs, we find a median, uncorrected for reddening, of $\langle M_H \rangle = -25.3 \pm 0.7$ with standard deviation $\sigma_{M_H} = 1.7$ for the M05 models, and when de-reddened by the median A_V , the median becomes $\langle M_H \rangle = -25.6$. There is thus no statistically significant difference in the typical M_H between the low- and high- z sub-samples. Both the low- and high- z sub-samples of SMGs have typical stellar luminosities which are greater than

local L^* galaxies ($M_H^* = -23.7$; Cole et al. 2001), which suggests that the stellar populations of SMGs are younger, that typical SMGs are more massive than local L^* galaxies, or some combination of the two. Given that we observe these SMGs at high redshift, it is highly likely that their stellar populations are younger than those of old local L^* galaxies, but we should compare the stellar masses of SMGs to those of L^* galaxies directly to examine the effect of mass.

4.3. Stellar Mass Results for SMGs

As mentioned in §3.2, we have chosen a stellar mass estimation procedure which constrains the average over the entire sample at the expense of accuracy in the mass of the individual galaxies. As a result, although we list stellar masses for individual SMGs in Table 2 for readers who wish to use them in spite of their uncertainty (factor of ~ 2 ; see §3.2), we do not wish to focus on results in an individual sense. We find it more appropriate to discuss the average (median/mean) mass of the sample and its range, which are not as sensitive to the star formation history uncertainty due to our large sample size. In Figure 10 we show the distribution of M_* for the $z > 1.5$ SMGs in our sample for both the M05 and the BC03 models to visually display the range in stellar mass of our sample. We caution that we have included in the histograms the stellar masses even for SMGs whose rest-frame optical and/or near-IR flux appeared to be dominated by a PL component prior to its removal, and remind the reader that the M05 stellar mass estimates use a different IMF (that of Kroupa 2001) from the BC03 stellar mass estimates (that of Chabrier 2003). While the distributions for the M05 and BC03 models have similar widths, $\sigma \sim 0.4$ dex, the distribution of BC03 stellar masses is shifted relative to the distribution of M05 masses such that, even when corrected to the same IMF, the M05 masses are systematically $\sim 20\%$ lower than the BC03 masses on average. We attribute at least some of the difference in the masses estimated using the M05 and BC03 models to the effects on the L_H/M_* ratio of TP-AGB stars included in the models of M05. At the average age of SMGs in the CSF model for M05, 1.6 Gyr, the L_H/M_* ratio is $\sim 40\%$ higher than that for the BC03 models at the average SMG age, 1.5 Gyr. We adopt the masses from the M05 models for the remainder of our discussion since the inclusion of the TP-AGB phase in stellar evolution in those models makes them more likely to be representative of the actual L/M ratio.

The median of the stellar mass distribution for the $z > 1.5$ SMG sample is $\langle M_* \rangle = (7.2 \pm 1.2) \times 10^{10} M_\odot$ for the M05 models [$\langle M_* \rangle = (9.0 \pm 1.7) \times 10^{10} M_\odot$ for the BC03 models]. The inter-quartile range (25th – 75th percentile) is $3.3 \times 10^{10} - 1.3 \times 10^{11} M_\odot$, suggesting that the $z > 1.5$ SMGs span a range of approximately an order of magnitude in stellar mass. The $z < 1.5$ SMGs in our sample seem slightly less massive on average than the high- z SMGs, having a median stellar mass of $\langle M_* \rangle = (4.4 \pm 1.7) \times 10^{10} M_\odot$ for the M05 models; however, the difference in median mass between the low- z and high- z SMGs is only $\sim 2\sigma$, and so not statistically significant. We note that the new median M_* we obtain for the $z > 1.5$ SMGs lies between that of model $z \sim 2$ SMGs in the semi-analytic model examined in Swinbank et al. (2008, $M_* = 2.1 \times 10^{10} M_\odot$) and the model SMGs in the hydrodynamical simulations of Davé et al. (2010, $M_* = 2.7 \times 10^{11} M_\odot$); thus our new estimate does not favor one set of theoretical models over the other. We also note that the median stellar mass we obtain here for $z > 1.5$ SMGs does not qualitatively

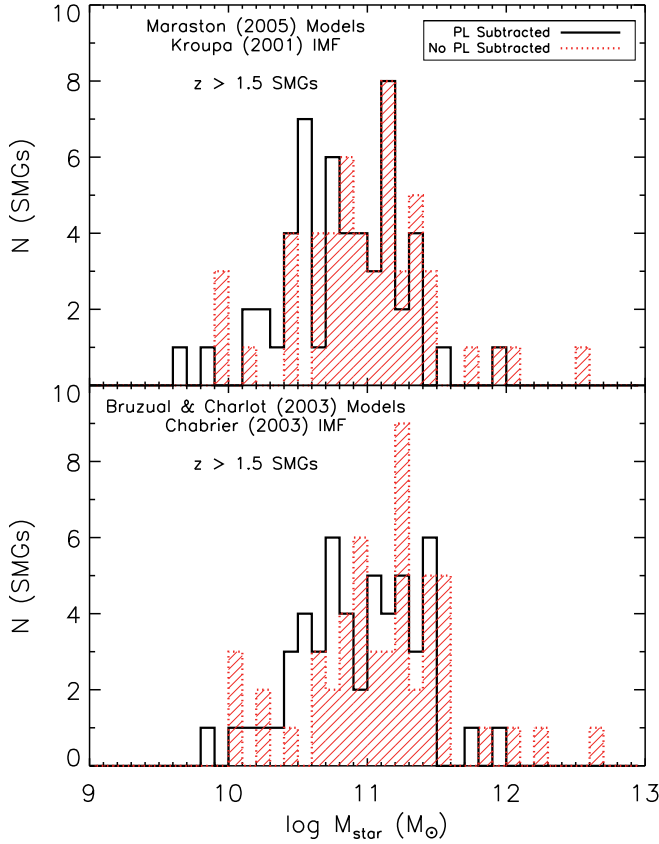


Figure 10. Histograms of stellar mass (M_*) for C05 sample of SMGs using the stellar population synthesis models of M05 (top) and BC03 (bottom). The filled histogram indicates the M_* distribution when no power-law component is subtracted as part of the SED fitting; in those distributions a slight shift to higher M_* can be observed. The distributions span approximately an order of magnitude, and the power-law-subtracted distributions have medians $(7.2 \pm 1.2) \times 10^{10} M_\odot$ (M05 models) and $(9.0 \pm 1.7) \times 10^{10} M_\odot$ (BC03 models).

change the conclusion of Alexander et al. (2008a) that the majority of SMGs fall a factor of 3–5 below comparably massive local galaxies on the $M_{BH} - M_*$ relation; thus, any lag in the growth of the central black holes relative to the host galaxy is modest in SMGs.

The typical stellar mass of SMGs found in previous observational studies span an order of magnitude; our new result is intermediate between the estimate of Smail et al. (2004, $M_* \sim 3 \times 10^{10} M_\odot$), who lacked rest-frame near-IR data for their analysis and thus could only weakly constrain the stellar mass, and the results of previous studies which used rest-frame near-IR data from *Spitzer*-IRAC (Borys et al. 2005; Dye et al. 2008; Michałowski et al. 2010). Although lower, our median M_* is marginally consistent with that obtained by Borys et al. (2005, $\langle M_* \rangle = 3.3 \pm 1.2 \times 10^{11} M_\odot$), whose SMG sample is contained fully within ours, falling just outside their $\pm 2\sigma$ uncertainty interval. A better comparison to Borys et al. is to compute the median M_* for only the subsample of SMGs which were also studied by those authors; when we do so, we obtain $\langle M_* \rangle = (1.3 \pm 0.3) \times 10^{11} M_\odot$, which falls within the $\pm 2\sigma$ uncertainty interval of Borys et al.. We note that since the stellar population models we have used for our study are not available for the IMF used by Borys et al., that of Miller & Scalo (1979), we cannot make a precise comparison between the two results; however, the smaller contribution

of low mass stars in the Miller & Scalo (1979) IMF relative to the Kroupa IMF suggests that the discrepancy in the median between the two studies may be somewhat larger under the Miller & Scalo (1979) IMF. To compare our new result to those of Dye et al. (2008) and Michałowski et al. (2010), who use a Salpeter IMF, we have also carried out our SED fits with a Salpeter IMF and find that our median mass for $z > 1.5$ SMGs increases to $1.3 \times 10^{11} M_\odot$. Despite the increase resulting from the IMF conversion, our typical stellar mass is still significantly smaller than that found by Dye et al. (2008, $\langle M_* \rangle = 6.3^{+1.6}_{-1.3} \times 10^{11} M_\odot$), falling outside their $\pm 3\sigma$ uncertainty interval. Michałowski et al. (2010) obtain a median stellar mass of $\langle M_* \rangle = 3.5 \times 10^{11} M_\odot$, a factor of 2.7 larger than our median M_* ; the significance of the difference is unclear since Michałowski et al. provide no uncertainty estimates for their individual or median stellar masses.

While the fact that we have used different stellar population models (e.g., Borys et al. 2005 use the stellar population models of Bruzual & Charlot 1993) likely plays a role in our systematically lower stellar mass estimates, the uncertainties associated with the different models are insufficient to fully account for the discrepancies. One important factor underlying our smaller stellar mass estimates is that we do not assume that the near-IR light from SMGs is entirely stellar in origin, unlike the studies of Borys et al. (2005) and Dye et al. (2008). Rather, we have subtracted the non-stellar near-IR excess from the observed photometry and used M_H to calculate the stellar mass instead of M_K since the contribution of the power-law emission is lower in the H -band than in K -band. If we instead estimate M_* for our sample using rest-frame K -band absolute magnitudes and *do not* subtract the near-IR excess, the median mass for our sample is $\langle M_* \rangle = 1.3 \times 10^{11} M_\odot$ under the M05 models and Kroupa IMF, a factor of ~ 2 higher, reflecting the impact of the near-IR continuum excess on the stellar masses in an average sense. We thus expect that the previous studies in which the near-IR continuum excess was not subtracted prior to stellar mass calculation have systematically overestimated the stellar masses of SMGs with near-IR excesses.

In §4.2 above we noted that typical SMGs have brighter stellar M_H than local L^* galaxies, which could be due to a higher stellar mass in SMGs or younger stellar population ages. It is thus notable that we find that the typical stellar mass of high- z SMGs is a factor of 2 *below* the typical stellar mass of local L^* galaxies ($m^* \sim 1.4 \times 10^{11} M_\odot$; Cole et al. 2001). Thus, the difference in stellar M_H between SMGs and local L^* galaxies can be attributed to the younger stellar population ages of SMGs. We note, though, that given the systematic errors in our mass estimates, which we discussed earlier in §3.3, we consider the typical stellar mass of high- z SMGs to be roughly consistent with m^* . We will return to the comparison of SMGs with local galaxies in §5.4.

4.4. Average Extinction of the Stellar Populations of SMGs

Our stellar population model fitting, which assumes a simple dust screen model, also provides estimates of the typical V -band extinction for our sample of SMGs. Because the SMGs are unresolved in their observed-frame optical-IRAC photometry, we regard these extinctions as averages across the entire galaxy; the true obscuration probably varies with location. However, since the extinction estimates are correlated with stellar population age and star formation history, which we could not firmly constrain for individual SMGs,

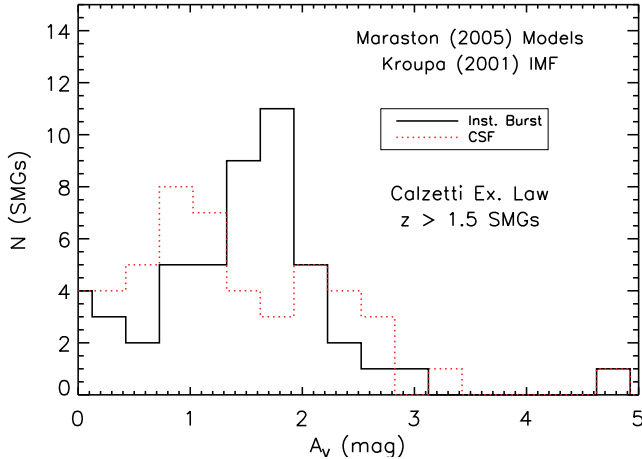


Figure 11. Histograms of A_V for C05 sample of SMGs using the stellar population synthesis models of M05 for two different choices of star formation history, assuming the Calzetti et al. (2000) extinction law for starburst galaxies. The total near-IR light we observe from SMGs is only modestly extinguished, having median $\langle A_V \rangle = 1.2 - 1.5$, depending on the choice of star formation history.

we once again consider the average and range over the entire sample to be the best-constrained quantities. We show the distribution of the fitted extinctions for both IB and CSF star formation histories for $z > 1.5$ SMGs in Figure 11, which illustrate both the likely range of A_V over the sample and the effect of star formation history on the extinction estimates. The distributions for both star formation histories indicate that the galaxy-averaged optical and near-infrared light that we detect from high- z SMGs is typically moderately obscured ($0.5 < A_V < 1.5$), with medians of $\langle A_{V,burst} \rangle = 1.5 \pm 0.1$ mag and $\langle A_{V,CSF} \rangle = 1.2 \pm 0.2$ mag and standard deviations of 0.8 and 1.0 mag, respectively. The extinction in the $z < 1.5$ sub-sample spans a similar range, with medians $\langle A_{V,burst} \rangle = 1.6 \pm 0.2$ mag and $\langle A_{V,CSF} \rangle = 1.8 \pm 0.3$ mag and standard deviations of 0.8 and 0.7 mag. To give the reader a sense of the difference in A_V between star formation histories for individual SMGs, the values we list in Table 2 are the average of the A_V 's found for the CSF and IB star formation histories, and the errors are taken to be half the difference between the two. The typically modest visual extinctions we obtain are consistent with those estimated from the Balmer decrement (Takata et al. 2006), but contrast sharply with the extreme IR luminosities of SMGs, which imply powerful energy sources hidden behind copious dust, and with the typical visual extinction derived from the optical depth of the $9.7 \mu\text{m}$ silicate absorption feature in the mid-IR spectra of SMGs ($A_V \sim 6$; Menéndez-Delmestre et al. 2009). However, we may reconcile the optical/near-IR A_V estimate with the mid-IR estimate by noting that the mid-IR light is less sensitive to dust extinction so we receive emission from more obscured regions at mid-IR wavelengths than at optical wavelengths, thus increasing the average A_V we derive.

The discrepancy between optical and mid-IR estimates of A_V highlights the difficulty in quantifying the stellar mass behind heavily obscured star formation complexes by means of an UV-near-IR SED fitting analysis, and again we caution that such mass may be missing from our estimates in this paper. How much the mass has been underestimated depends critically on the dust distribution in SMGs, which remains poorly known. If the star forming clouds and heavy extinction are patchy and distributed over the galaxy, then older stars will

eventually diffuse out of the heavily obscured regions (perhaps on Milky-Way-type time-scales of ~ 100 Myr). In this case, we would be able to observe the bulk of the stellar mass, except in the earliest formation stages of the galaxy. On the other hand, if the entire galaxy is enshrouded in dust, and the older stars never diffuse out to regions of lower extinction, a large fraction of the stellar mass could be hidden. While comparisons with dynamical mass estimates of SMGs (see §5.1) suggest that a large fraction of the stellar mass is not missing from our estimates, the dynamical masses are derived using a tracer (gas) which may not have the same spatial distribution as the stars and may not be representative of entire galaxies.

5. DISCUSSION

In this section we combine the stellar luminosities and typical stellar mass we have derived for our SMG sample with various mass, AGN, and star formation indicators to extract their implications for the nature of SMGs and their future evolutionary path. We first perform a small, but independent, check of our typical stellar mass estimate to evaluate its plausibility before moving on to perform comparisons of SMGs to other populations of high- z galaxies. We will also discuss the origin of the non-stellar near-IR continuum emission. Finally, we will use constraints from the fading over time of stellar population models to predict the $z = 0$ descendants of SMGs.

5.1. Comparison to Dynamical Mass from CO Observations: Testing M_*

The various different systematic uncertainties associated with stellar mass determinations, and the different results which have been obtained in the literature strongly highlight the need for independent checks on stellar mass estimates. In principle, the best check on any stellar mass estimate is to compare M_* to the dynamical mass, M_{dyn} . However, Greve et al. (2005) warn that the dynamical masses of SMGs must be treated with caution, because M_{dyn} for SMGs (and other galaxies) is usually calculated assuming the system is in dynamical equilibrium and that we know the velocity field and mass distribution, whereas SMGs may be the product of a merging gas-rich system (e.g., Smail et al. 1998, 2004; Tecza et al. 2004; Swinbank et al. 2006; Tacconi et al. 2008) which is not in dynamical equilibrium. If the system is not in dynamical equilibrium, the mass distribution assumed is incorrect, or if the observed CO line is not a good tracer of the system dynamics or mass, M_{dyn} will be different. Moreover, high-resolution millimeter observations by Tacconi et al. (2006, 2008) and Bothwell et al. (2010) suggest that the CO-emitting region ($R \sim 1 - 2$ kpc) in SMGs is frequently smaller than the overall stellar mass and star formation distribution (Chapman et al. 2004; Biggs & Ivison 2008; Swinbank et al. 2010), so the dynamical masses from CO observations are often lower limits. A further complication is that the dynamical mass is not exclusively a baryonic mass: since a galaxy's dark matter halo contributes to the gravitational potential and thus to the velocity field, the galaxy's mass derived from the velocity field will contain some contribution from dark matter. The fractional contribution of dark matter to the available CO dynamical mass estimates is currently unknown; however, the likely descendants of SMGs in the local universe (i.e., galaxies of equal or greater stellar mass) have been observed to be baryon-dominated on scales similar to the CO-emitting region in SMGs (e.g., Gerhard et al. 2001; Cappellari et al. 2006; Kassin et al. 2006; Williams et al. 2009).

In spite of the uncertainties, we use the 16 SMGs with CO observations in our sample to carry out the best test available of the stellar masses we have derived. We list the molecular gas results and dynamical mass estimates for the 16 SMGs which have published CO observations in Table 4, noting that only the CO-detected SMGs have estimates of M_{dyn} . Tacconi et al. (2008) have carried out a comparison of gas, stellar, and dynamical mass for four of the SMGs in our sample already, in order to constrain the IMF and CO-to- H_2 conversion factor for high- z galaxies, and found that the stellar masses of two of the SMGs exceeded the dynamical mass. However, we are more concerned here in determining if the typical stellar mass of SMGs is consistent with the typical dynamical mass, since our stellar masses for individual SMGs are highly uncertain. The median dynamical mass for SMGs in our sample with CO observations is $\langle M_{\text{dyn}} \rangle = 2.3 \times 10^{11} M_\odot$ and thus consistent with the sum of the median stellar mass ($M_\star = 7.2 \times 10^{10} M_\odot$) and the median molecular gas mass [$M(\text{H}_2) = 3.0 \times 10^{10} M_\odot$] of the SMGs with CO observations (which is identical to the median of the combined samples of Greve et al. 2005; Tacconi et al. 2006, 2008). Thus, assuming the median M_{dyn} and $M(\text{H}_2)$ are representative of the whole sample, we conclude that our median stellar mass estimate is generally consistent with the published dynamical masses of SMGs.

5.2. The Origin of the Near-IR Continuum Excess in SMGs

Although the majority of our SMG sample does not contain a dominant near-IR PL component, we nevertheless wish to understand the origin of the near-IR excess observed in a significant fraction of the galaxies in our sample. To test the origin we need to distinguish the near-IR emission from the galaxies' nuclei from that which follows the obscured star formation (which may be more distributed; see, e.g., Chapman et al. 2004; Biggs & Ivison 2008; Menéndez-Delmestre et al. 2009). Yet, because high- z SMGs are unresolved in our IRAC images, we cannot directly connect the PL emission to the galaxies' nuclei or star formation regions; we must find some other means of discriminating between the central SMBH and the host galaxy as the source of the near-IR excess. One way to do so is to examine other AGN indicators in the SMGs: if the origin of the excess is AGN, we would expect that the presence and/or luminosity of a significant PL component correlates with other AGN signatures, unless the AGN is highly obscured and Compton-thick (which does not appear to be the case for the majority of SMGs; see Alexander et al. 2005).

The hard X-ray luminosity of a galaxy is regarded as one of the best tracers of SMBH activity for Compton-thin nuclei, since the hard X-rays are less susceptible to the heavy obscuration thought to enshroud a central SMBH. Moreover, numerous authors have shown that the hard X-ray luminosity of QSOs and Seyfert 1 galaxies is correlated with the nuclear near-IR luminosity (e.g., Carleton et al. 1987; Alonso-Herrero et al. 1997; Mushotzky et al. 2008), who frequently conclude that the non-stellar near-IR (e.g., K , L , and M bands) emission originates from hot dust heated by the AGN. 23 SMGs in our sample have rest-frame hard X-ray data available in the literature (Alexander et al. 2005, 2008a; Le Floch et al. 2007). For these galaxies we can most directly test if the near-IR excess is associated with an AGN, by checking if the hard X-ray luminosity correlates with the luminosity in the near-IR PL component. Although the most

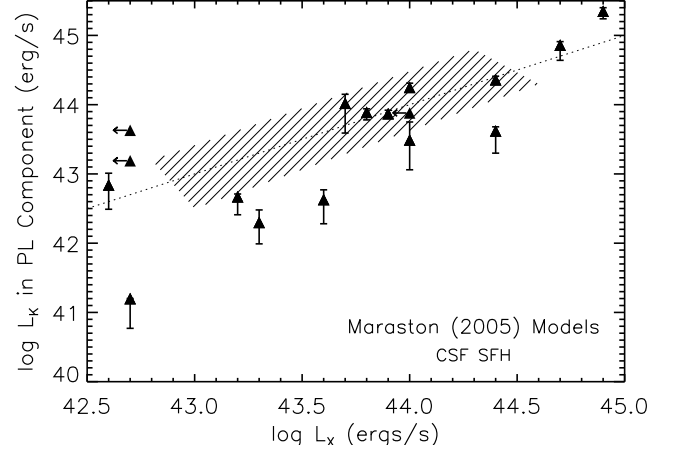


Figure 12. Rest-frame K -band luminosity in the PL component as a function of extinction-corrected X-ray luminosity for the SMGs which have X-ray observations in the literature. The dotted line represents $L_K(\text{PL Component}) = L_X$. The shaded area shows the region in which local AGN fall. With the exception of 2 SMGs which may be Compton-thick AGN, and 3 SMGs which have no near-IR PL component, L_X is clearly correlated with the K -band luminosity of the non-stellar continuum excess; the correlation suggests that AGN are the origin of the near-IR continuum excess in SMGs.

significant correlations in local AGN samples between near-IR and X-ray emission occur in L and M bands due to stellar contamination in bluer bands, our IRAC data cannot constrain bands redward of rest-frame K for most of our sample. Thus, to test for a correlation, we have calculated the rest-frame K -band luminosity contained within the PL component for each of the 23 SMGs with X-ray data (in addition to computing the same for rest-frame H -band in §4.1). In Figure 12 we show the absorption-corrected X-ray luminosity (L_X) versus the rest-frame K -band luminosity (L_K) of the PL component for the SMGs which have X-ray observations. Excepting 2 galaxies with low L_X and high L_K in the PL component, which may host Compton-thick AGN, and 3 galaxies which have no near-IR PL component and thus likely lack a hot dust component (similar to the local ULIRGs NGC 6240 and NGC 4945), L_K of the PL component is well-correlated with L_X . The correlation remains apparent even when we restrict the redshift range of the X-ray observed sample to $2.0 < z < 2.6$, indicating that the correlation is not merely an artifact of galaxy distance. The median ratio of the K -band PL luminosity and L_X for all of the SMGs with X-ray data, $L_K(\text{PL})/L_X = 0.9 \pm 0.4$ with RMS scatter 1.9, is not dissimilar to the L_K/L_X ratio of the average radio-quiet QSO SED from Elvis et al. (1994) ($L_K/L_X \sim 0.4$), and the range spans those observed for local PG QSOs, Seyfert 1s, and Seyfert 2s (e.g., Alonso-Herrero et al. 1997).

The observed $L_X - L_K$ correlation for our SMGs with X-ray data and the similarity of their L_K/L_X ratios to local obscured and unobscured AGN indicate a probable AGN origin of the near-IR excess for the galaxies in which the excess is present in the K -band. To lend credibility to this conclusion we also examine the spectroscopic classifications of the SMGs which have significant near-IR PL contributions. When we search through the rest-frame UV, $H\alpha$, mid-IR, and X-ray spectral classifications available for the SMGs in our full sample, we find that, of the 25 SMGs which have fractions of rest-frame H -band PL-component luminosity greater than 0.2, 20 have been classified as AGN. The remaining 5 have starburst classifications, but the only available spectroscopic data is from the

rest-frame UV, which is very sensitive to dust obscuration and thus is not a reliable indicator of AGN activity¹⁴. Thus, the spectroscopic classifications of the SMGs in our sample with significant PL components are generally consistent with an AGN origin for the near-IR continuum excess in those galaxies. However, for the SMGs which are at $z < 1.8$ and show a near-IR excess only in one appropriate photometric band, we cannot rule out a contribution from a $3.3\ \mu\text{m}$ PAH emission line without spectroscopic data. We note that SMGs in our sample without a near-IR excess do not universally lack an AGN spectral identification: in fact, $\sim 60\%$ of the galaxies without a near-IR excess have been identified as AGN through spectroscopy at some wavelength. However, as we mentioned in the previous paragraph, some local AGN lack hot dust components; thus, the presence of AGN in SMGs without a near-IR excess does not render invalid our conclusion for SMGs with significant excess near-IR emission.

Since such a large fraction of our SMG sample ($\sim 70\%$; see §3.1.2) display this near-IR excess which seems to be associated with AGN (at least in the galaxies with the strongest PL contribution), it is interesting to determine if the frequency of near-IR continuum excess observed in our sample is similar to that of independent SMG samples. One completely independent SMG sample we can compare to is that catalogued in the Extended-*Chandra* Deep Field-South (E-CDFS) by Weiß et al. (2009). To reduce the effect of spectroscopic bias from our comparison, we examine the number of SMGs in each sample displaying a near-IR excess relative to the full number of SMGs in the parent sample, including those whose radio or mid-IR counterparts were not identified. Wardlow et al. (2011) find that 13 out of the parent sample of 126 SMGs in the E-CDFS show a non-stellar excess at observed-frame $8.0\ \mu\text{m}$ ($\sim 10\%$), whereas for our sample 44 galaxies out of the parent sample of 150 SMGs in C05 display non-stellar excess in their IRAC photometry ($\sim 30\%$). The large difference in frequency of near-IR excess suggests that some bias towards hot dust emitters and AGN exists in the C05 SMG sample. Some bias toward AGN in the C05 sample could have arisen through the spectroscopic selection, in that SMGs with multiple emission lines in their spectra were more likely to be identified than, for example, galaxies with one (or no) emission line. However, future submillimeter surveys in additional sky fields are required to confirm that the C05 SMG sample suffers from an AGN selection bias.

5.3. Comparison of SMGs to Other High- z Galaxy Populations

In Paper I we compared the rest-frame near and mid-IR colors of SMGs to the samples of stellar-dominated, rest-frame-UV-selected, $z \sim 3$ Lyman-break galaxies (LBGs) and $z \sim 2$ BX/BM galaxies from Reddy et al. (2006) and the radio-loud, obscured AGN-dominated high- z radio galaxies (HzRGs) from Seymour et al. (2007), all of which have spectroscopic redshifts. Our comparisons indicated the SMGs are brighter and redder than UV-selected galaxies at high- z , suggesting that they have higher mass, extinction, and possibly hot dust contribution. SMGs are similarly bright and red as HzRGs, suggestive of similar mass and hot dust contribution. Now we have stellar luminosities and a median stellar

mass for the SMG sample and thus we can compare the stellar components of the high- z populations directly. As in Paper I, we prefer to compare only to galaxy samples with spectroscopic redshifts to eliminate uncertainty associated with redshift; we thus use the same comparison samples of LBGs, BX/BM galaxies, and HzRGs as in Paper I. For the present study we now also include the $z \sim 2$ K -selected galaxies (distant red galaxies, or DRGs) with spectroscopic redshifts from Kriek et al. (2006, 2007, 2008), to broaden our range of high- z comparison galaxy populations. We note that each sample of galaxies representing each population have been selected by different criteria and at different wavelengths, and thus each suffers from different selection effects which are beyond the scope of this paper to analyze. As in Paper I, our comparison is not intended to be comprehensive or representative; we merely wish to obtain an idea of the relationships between well-studied galaxy samples.

Looking at the median rest-frame H -band absolute magnitudes for the various types of high- z galaxies, we find that the typical DRG, SMG, and HzRG are ~ 2 or more magnitudes brighter than the typical LBG or BX/BM galaxy. The reddening-corrected median M_H values for DRGs, SMGs, and HzRGs are -26.2 ± 0.1 (A. Muzzin, private communication), -26.0 ± 0.2 , and -25.7 (Seymour et al. 2007), respectively, while the median M_H for the LBGs and BX/BM galaxies in the Reddy et al. (2006) sample are -23.8 ± 0.2 and -23.6 ± 0.1 , respectively. The $\sim 2 - 2.5$ mag difference between the UV-selected galaxies and the DRGs, SMGs, and HzRGs is statistically significant in all cases where a bootstrapped error in the median is available, and corresponds to a factor of $\sim 6 - 10$ in luminosity. The difference in near-IR stellar luminosity probably reflects a lower stellar mass in LBGs and BX/BM galaxies, for three reasons: (1) the hot dust contribution to M_H has been removed from the SMGs and HzRGs; (2) the UV-selected galaxies are less obscured, so extinction is unlikely to be a factor in the lower M_H ; and (3) because we receive UV flux from young stars in UV-selected galaxies, it is unlikely that the dominant stellar populations in LBGs and BX/BM galaxies are older (and thus fainter) than in the DRGs, SMGs, and HzRGs. The smaller differences in M_H among DRGs, SMGs, and HzRGs, however, are less clear in origin but are usually not statistically significant. Hence, we conclude that DRGs, SMGs, and HzRGs have essentially similar stellar near-IR luminosities, and possibly stellar masses.

Our next step should be to compare the stellar masses of the SMGs, LBGs, DRGs, HzRGs, and BX/BM galaxies. Due to the various systematic uncertainties associated with M_* estimates made through fitting stellar population synthesis models, our preference is to compare galaxy samples whose mass estimates have been derived in a consistent manner. However, no such concordance exists in the literature at this moment between the stellar mass-estimating methods of the high- z galaxy types selected through different criteria.

In the absence of consistently-derived stellar mass estimates in the literature for different high- z populations, we have chosen to apply our stellar population model plus power law SED fitting technique to the sample of UV-selected galaxies in Reddy et al. (2006) and derive stellar masses for that sample in the same manner as we have done for the SMGs in our sample. We have chosen to use the LBGs and BX/BM galaxies in Reddy et al. (2006) because complete optical, near-IR, and IRAC photometry are readily available for a large number of galaxies, along with spectroscopic redshifts. The median stellar masses we calculate from our method are $\langle M_* \rangle = (7.7 \pm$

¹⁴ As an illustration of the capability of the rest-frame UV spectra to be misleading, we note that the two SMGs which do not follow the $L_X - L_K$ relation and could host Compton-thick AGN have starburst classifications in the rest-frame UV, but are continuum-dominated in their mid-IR spectra from IRS.

$0.2) \times 10^9 M_\odot$ for LBGs and $\langle M_\star \rangle = (5.9 \pm 0.1) \times 10^9 M_\odot$ for the combined BX/BM sample, which are roughly consistent with the stellar mass estimates of Reddy et al. (2006) when scaled to the Kroupa (2001) IMF. When we compare the median stellar mass of SMGs, $\langle M_\star \rangle = 7.2 \times 10^{10} M_\odot$, to the self-consistently calculated median stellar masses of the UV-selected galaxies, we unambiguously determine that the UV-selected galaxies are approximately an order of magnitude less massive than SMGs. Such a disparity in mass does not, however, rule out $z \sim 2$ SMGs as direct evolutionary descendants of UV-selected galaxies at $z \sim 3$, because, assuming LBGs contain the necessary quantity of molecular gas, the time to form the stellar mass of a typical $z \sim 2$ SMG from the typical mass of a typical LBG at the typical LBG star formation rate ($\sim 50 M_\odot \text{ yr}^{-1}$; Kornei et al. 2010) is ~ 1 Gyr, roughly the separation in cosmic time between $z \sim 2$ and $z \sim 3$.

5.4. The Future Evolution of SMGs

We have now established the typical stellar content of SMGs at $z \sim 2$; yet we still wish to understand what form the descendants of SMGs will have in the local Universe. To explore the future evolution of SMGs after the termination of the starburst we can employ simple stellar evolution models based on these star formation time-scales and use the models to predict the stellar luminosity distribution of the descendants of SMGs from their M_H distribution at $z \sim 2$. For the purposes of our discussion here, since we could derive no constraints on star formation history from our SED fits (see §3.1.1), we conservatively assume a simple scenario in which we observe the $z \sim 2$ SMGs in the middle of last major starburst event in their history; after the burst ends, they will not undergo subsequent mergers or accretion and the stars will evolve passively. Our scenario thus provides a lower limit on the likely $z = 0$ luminosity of SMG descendants.

We first construct the high- z M_H distribution for our sample of $z > 1.5$ SMGs using the power-law continuum-subtracted (stellar) values of M_H which have been individually dereddened and averaged between the IB and CSF star formation histories. The final distribution, shown in Figure 13 as the solid histogram, has median $\langle M_H \rangle = -26.0 \pm 0.2$. We note that we do not exclude from the stellar M_H distribution the SMGs which have significant ($> 50\%$) PL components, although their stellar M_H values probably have large uncertainties. Then, we evolve our sample of $z > 1.5$ SMGs to the present day using the M05 stellar population synthesis models with a Kroupa (2001) IMF. We consider as possible scenarios that SMGs are starbursts of constant SFR of duration 50, 100, 200, and 400 Myr, covering the range of estimates of the duration of the starburst in the SMG phase from CO observations (e.g., Neri et al. 2003; Greve et al. 2005; Tacconi et al. 2006). We assume that we observe each SMG halfway through its star formation burst, and then compute the fading that occurs between ages 25, 50, 100, and 200 Myr and 10 Gyr (roughly the difference in cosmic time between $z \sim 2$ and $z = 0$). The faded luminosity distributions for each burst duration are shown as the dotted histogram in Figures 13 and 14, and predict median stellar absolute H magnitudes for the SMGs at $z = 0$ of $M_H = -22.1, -22.6, -23.1$, and -23.6 , respectively, for burst durations of 50, 100, 200, and 400 Myr. We observe that the predicted median values of M_H are all fainter than L^* at $z = 0$ ($M_H^* = -23.7$; Cole et al. 2001); however, recall that these predictions are conservative lower limits. Subsequent mergers or

star formation can increase the mass and luminosity of SMG descendants by varying factors, and may reasonably be expected.

We can put these aged and faded SMGs into context by comparing them to a sample of massive elliptical galaxies in the local Universe. We use as our local massive elliptical galaxy sample the ellipticals in the Coma cluster since they have a large, homogeneous, near-IR photometry data set and optical morphology data set. We construct the M_H distribution for massive ellipticals in Coma using H -band 2MASS photometry and optical morphologies compiled by R. Smith and J. Lucey (2009, private communication). To convert the observed H magnitudes to M_H , we use a distance modulus $m - M = 35.0 \text{ mag}$ (e.g., Liu & Graham 2001). We include the M_H distribution of Coma ellipticals in Figures 13 and 14 as the dashed histogram. Somewhat surprisingly, the SMG distributions faded for 50, 100, and 200 Myr bursts all reasonably match the Coma M_H distribution within $\sim 0.5 \text{ mag}$: two-sided Kolmogorov-Smirnov (K-S) tests comparing to Coma distribution to each of the faded SMG distributions produce probabilities of being drawn from the same parent distribution of 1.3%, 35%, and 13%, respectively, so we cannot distinguish any of these faded distributions from the Coma ellipticals. (We note that the 400 Myr burst distribution, when compared to the Coma distribution in the K-S test, produces a probability of 0.07%.) As shown in Figure 13, the SMG distribution faded according to the 100 Myr burst model appears to best match the distribution of the Coma cluster ellipticals, although the differences between the 50, 100, and 200 Myr burst models applied to the SMG distribution are probably not significant. Our comparison of the M_H distribution of the elliptical galaxies in the Coma cluster to faded M_H distributions for $z > 1.5$ SMGs thus suggests that, for reasonable starburst durations (50–200 Myr), and under the conservative assumption of no significant growth in stellar mass after the SMG phase terminates, the $z = 0$ SMG descendants may be massive elliptical galaxies with a luminosity (and therefore mass) distribution similar to that of massive ellipticals in the Coma cluster (the majority of which fall in the range $0.2L^* - 2L^*$). We note that this range is somewhat lower than the luminosity of present-day SMG descendants estimated by Swinbank et al. (2006, $\gtrsim 3L^*$) by comparing the average velocity dispersion of 5 SMGs to the present-day Faber-Jackson relation. In light of the uncertainty in both analyses (arising from star formation history assumptions in this paper and the assumptions of virial equilibrium and no evolution in velocity dispersion by Swinbank et al.), the two results may be reconcilable. However, our sample of SMGs is ~ 10 times larger than that of Swinbank et al. (2006), and therefore is likely more representative of the range of mass and luminosity among SMGs.

If burst durations of 50–200 Myr are indeed correct for SMGs, then it is interesting to determine from them what fraction of today's massive ellipticals underwent a SMG phase. We can use the starburst durations which predict the SMG fading that best matches the Coma ellipticals to estimate the space density of SMG descendants of similar luminosity/mass to Coma ellipticals, and see how that compares to the space density of similar ellipticals from local galaxy luminosity functions. We calculate the space density of SMG descendants assuming each galaxy goes through only one SMG phase using the simple relation

$$\phi_D = \rho_{\text{SMG}} (t_{\text{obs}}/t_{\text{burst}}), \quad (2)$$

where ϕ_D is the comoving space density of the descendants

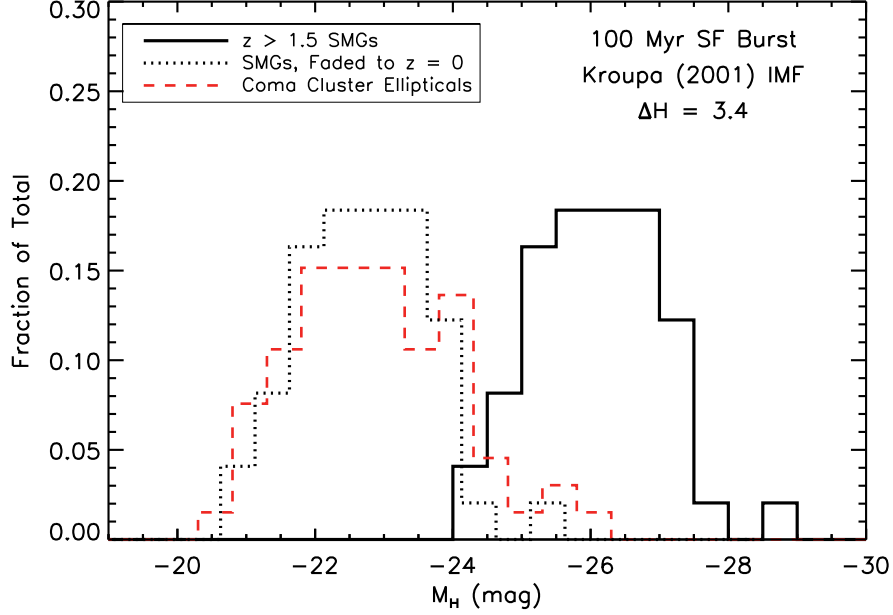


Figure 13. Comparison of the absolute H magnitude (M_H) distribution of the elliptical galaxies in the Coma cluster to that of the stellar component of our spectroscopically-identified SMGs at $z > 1.5$. The distributions match well if we passively evolve the stars in SMGs to an age of 10 Gyr, modeling the SMGs as 100-Myr-long starburst events which, at $z \sim 2$, we observe halfway through at an age of 50 Myr. The match between the faded SMG distribution and the present-day Coma distribution suggests that, for the predicted time-scale of the starburst phase in SMGs, SMGs will evolve into galaxies of similar stellar luminosity and mass as the massive ellipticals in the Coma cluster if they evolve passively upon termination of the starburst.

of SMGs, ρ_{SMG} is the observed space density of SMGs, t_{obs} is the epoch over which we observe SMGs, and t_{burst} is the duration of the starburst. We determine t_{obs} from the redshift distribution for our SMG sample (updated from C05 with new results from Menéndez-Delmestre et al. 2009) after correcting for spectroscopic and radio detection incompleteness; similar to Swinbank et al. (2006), we use the $\pm 1\sigma$ interval around the median of the redshift distribution to define $t_{\text{obs}} \simeq 2.3$ Gyr. We estimate the observed space density of SMGs from the integral submm source counts for $S_{850} > 4$ mJy found by Coppin et al. (2006), $844 \pm 117 \text{ deg}^{-2}$, and the comoving volume between $z = 1.46 - 3.06$. In this way, the 50, 100, and 200 Myr starburst durations imply that the space density of SMG descendants at $z = 0$ will be $\phi_D \sim 2, 1, 0.5 \times 10^{-3} \text{ Mpc}^{-3}$. When we integrate the K -band luminosity function of early-type galaxies at $z = 0$ of Croton et al. (2005), we find that we can match the space density of SMG descendants of $\phi_D \sim 0.5 \times 10^{-3} \text{ Mpc}^{-3}$ by integrating the early-type luminosity function down to $1.3L^*$. For the 100 Myr-duration burst, we can match the predicted space density of $1 \times 10^{-3} \text{ Mpc}^{-3}$ if we integrate the early-type luminosity function down to $0.8L^*$. For the case of the 50 Myr-duration burst, we can match the predicted space density of $2 \times 10^{-3} \text{ Mpc}^{-3}$ by integrating the early-type luminosity function to $0.4L^*$. Thus, our calculations suggest that for starburst durations of 50–200 Myr, SMGs could account for the formation of the entire population of elliptical galaxies with luminosities greater than $\sim 0.4L^* - 1.3L^*$.

Given the systematic uncertainty associated with the form of the stellar IMF for high- z galaxies, our median stellar mass for $z > 1.5$ SMGs from §4.3 is essentially consistent with m^* , and is consistent with scenarios which predict that SMGs evolve into massive elliptical galaxies. Moreover, the baryonic masses (gas plus stars) of high- z SMGs, which serve as

an upper limit on the final stellar mass of SMGs assuming no future accretion or gas loss, also point toward a future for SMGs as $\sim m^*$ galaxies. Assuming the median molecular gas mass of CO-observed SMGs (from §5.1) is typical of our entire sample in an average sense, then the typical baryonic mass (gas plus stars) for our SMGs is $\langle M_{\text{baryon}} \rangle \sim 1.0 \times 10^{11} M_{\odot}$. This estimate excludes the contribution from neutral hydrogen; if we reasonably estimate that the contribution of neutral gas is similar to that in the Milky Way and thus equal to the mass of molecular gas, then the typical baryonic mass of SMGs would be $\langle M_{\text{baryon}} \rangle \sim 1.3 \times 10^{11} M_{\odot}$. Both estimates of baryonic mass closely resemble the stellar mass of a L^* galaxy in the local universe ($1.4 \times 10^{11} M_{\odot}$; Cole et al. 2001). On the other hand, feedback from star formation and/or AGN may result in outflows of gas from the galaxy so that only a fraction of the gas in SMGs at $z \sim 2$ is eventually converted to stars (e.g., Begelman 1985; Silk 1997; DiMatteo et al. 2005; Murray et al. 2010). Nevertheless, the baryonic mass is a strong indicator that the end product of the starburst phase in a typical SMG will be a galaxy of mass of order m^* at $z = 0$, within a factor of a few. Even considering the uncertainties, the baryonic mass is too small for typical SMGs to represent the formation phase of the very luminous, rare, cD-type galaxies observed in galaxy clusters; the space density of SMGs is also far too high to expect typical SMGs to all be so massive. As shown in Figure 10, a range of approximately an order of magnitude in stellar luminosity and mass does exist among $z \sim 2$ SMGs, including a high-mass tail, so some SMG descendants will evolve into massive ellipticals of $3L^*$ and up as predicted by Swinbank et al. (2006). Subsequent mergers or gas accretion will also produce more massive descendants. However, in the absence of significant mass accretion, the average SMG seems destined to be an $\sim L^*$ -type galaxy.

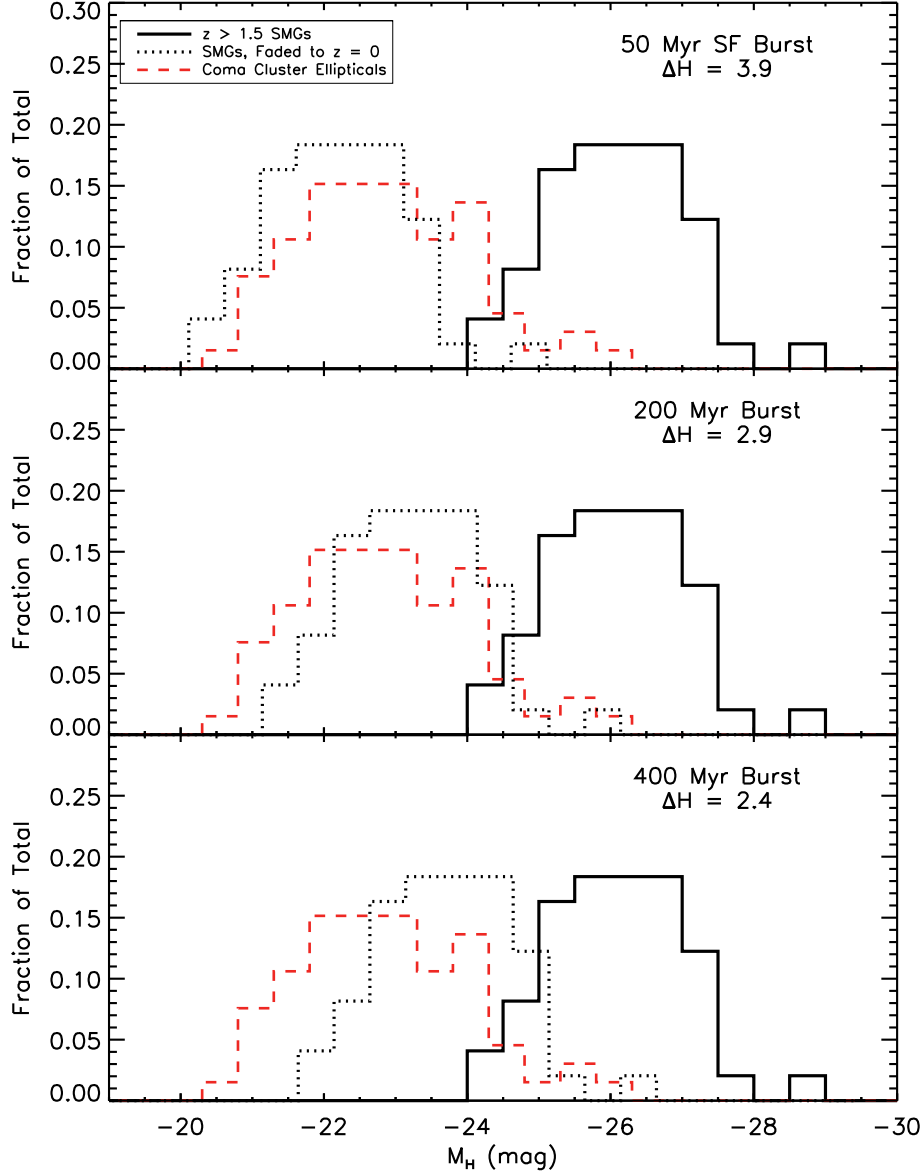


Figure 14. Comparison of the absolute H magnitude (M_H) distribution of the elliptical galaxies in the Coma cluster to that of the stellar component of our spectroscopically-identified SMGs at $z > 1.5$, assuming starburst lifetimes for the SMGs other than 100 Myr. The fading predicted by modeling SMGs as starbursts of duration 50 and 200 Myr cause the M_H distribution of SMGs to match the Coma cluster similarly as the 100 Myr burst; however, a 400 Myr burst duration will produce SMG descendants which are more luminous than is typical of the massive ellipticals in Coma.

In this paper we have fit the rest-frame UV through near-IR SEDs of the radio-detected SMGs with spectroscopic redshifts from Chapman et al. (2005) to estimate stellar masses. For the first time we remove the excess continuum contribution to the galaxies’ near-IR luminosity to ensure that we derive a mass for the stellar component only. Observing that the K -band luminosity of this near-IR excess is well-correlated with hard X-ray luminosity of the galaxy, we conclude that the near-IR continuum excess is caused by the galaxies’ AGN; however, for only 11% of our SMGs is the AGN contribution stronger than the stellar contribution in the rest-frame near-IR. In trying to fit synthetic stellar populations to our continuum excess-subtracted SEDs, we show that our photometric data spanning a broad range of wavelengths are still not sufficient to place useful constraints on the star formation history of the galaxies and, thus, the age of the dominant stellar pop-

ulations, since our galaxies are heavily reddened and our data are not well-enough sampled near the strong age indicators of the Balmer and 4000 Å breaks.

The median stellar mass of the galaxies in the sample is better constrained, however, despite systematic uncertainties. By taking a simple, physically motivated approach using a constant mass-to-light ratio, we find that SMGs have a modest median stellar mass of $7 \times 10^{10} M_\odot$, which is lower than most previous estimates of stellar mass in SMGs. Our new, lower stellar mass estimate for typical SMGs is consistent with the median dynamical mass of SMGs with CO observations. When we compare our typical SMG stellar mass to those of other high- z galaxy populations, the SMGs appear to be more massive by a factor of 10 than high-redshift UV-selected galaxies.

We then explore the possible evolution of SMGs after they

run out of molecular fuel for star formation, based on estimates in the literature for the gas consumption/starburst timescale in SMGs. We find that if we passively evolve SMGs to $z = 0$, the range of expected starburst time scales causes the rest-frame H absolute magnitude distribution of high- z SMGs to fade so that it nearly matches the M_H distribution of massive elliptical galaxies in the Coma galaxy cluster. The match to the Coma cluster distribution suggests that the descendants of typical SMGs will be $\sim m^*$ galaxies similar to Coma ellipticals in the local universe, and is further supported by the typical baryonic mass of our SMG sample ($\sim 10^{11} M_\odot$) which places an upper limit on the future stellar mass of SMGs assuming no further cold gas accretion. Thus, our results confirm the picture of high- z SMGs as highly luminous, massive galaxies simultaneously experiencing strong, obscured starburst activity and AGN activity fueled by massive molecular gas reservoirs, which will evolve into $\sim L^*$ -type galaxies following the exhaustion of their molecular gas.

We would like to thank the anonymous referee for helpful suggestions which improved the clarity of the paper. We thank C. Maraston for providing us with unpublished stellar population synthesis models, as well as C. Borys, P. Capak, and K. Bundy for helpful discussions on fitting stellar population models to observed SEDs. We thank M. Swinbank for helpful discussions as well. We wish thank R. J. Smith and J. R. Lucey for providing their compilation of morphologies and 2MASS photometry for the Coma Cluster. We acknowledge the use of the NASA Extragalactic Database, as well as E. L. Wright's web-based cosmology calculator. IRS acknowledges support from STFC. DMA acknowledges support from the Royal Society and the Leverhulme Trust.

REFERENCES

- Alexander, D. M., Bauer, F. E., Brandt, W. N., et al. 2003, *AJ*, 125, 383
- Alexander, D. M., Bauer, F. E., Chapman, S. C., et al. 2005, *ApJ*, 632, 736
- Alexander, D. M., Brandt, W. N., Smail, I., et al. 2008a, *AJ*, 135, 1968
- Alexander, D. M., Chary, R., Pope, A., et al. 2008b, *ApJ*, 687, 835
- Alonso-Herrero, A., Pérez-González, P. G., Alexander, D. M., et al. 2006, *ApJ*, 640, 167
- Alonso-Herrero, A., Quillen, A. C., Rieke, G. H., Ivanov, V., & Efstathiou, A. 2003, *AJ*, 126, 81
- Alonso-Herrero, A., Ward, M. J., & Kotilainen, J. K. 1997, *MNRAS*, 288, 977
- Barger, A. J., Cowie, L. L., Sanders, D. B., et al. 1998, *Nature*, 394, 428
- Baugh, C. M., Lacey, C. G., Frenk, C. S., et al. 2005, *MNRAS*, 356, 1191
- Begelman, M. C. 1985, *ApJ*, 297, 492
- Bell, E. F., & de Jong R. S. 2001, *ApJ*, 550, 212
- Biggs, A. D., & Ivison, R. J. 2008, *MNRAS*, 385, 893
- Blain, A. W., Chapman, S. C., Smail, I., & Ivison, R. 2004a, *ApJ*, 611, 52
- Blain, A. W., Chapman, S. C., Smail, I., & Ivison, R. 2004b, *ApJ*, 611, 725
- Blain, A. W., Smail, I., Ivison, R. J., & Kneib, J.-P. 1999, *MNRAS*, 302, 632
- Bolzonella, M., Miralles, J.-M., & Pelló, R. 2000, *A&A*, 363, 476
- Borch, A., Meisenheimer, K., Bell, E. F., et al. 2006, *A&A*, 453, 869
- Bouchet, P., Lequeux, J., Maurice, E., Prévot, L., & Prévot-Burnichon, M. 1985, *A&A*, 149, 330
- Borys, C., Smail, I., Chapman, S. C., et al. 2005, *ApJ*, 635, 853
- Bothwell, M. S., Chapman, S. C., Tacconi, L. J., et al. 2010, *MNRAS*, 405, 219
- Bower, R. G., Lucey, J. R., & Ellis, R. S. 1992, *MNRAS*, 254, 601
- Bruzual, G., & Charlot, S. 1993, *ApJ*, 405, 538
- Bruzual, G., & Charlot, S. 2003, *MNRAS*, 344, 1000
- Calzetti, D., Armus, L., Bohlin, R. C., et al. 2000, *ApJ*, 533, 682
- Capak, P., Cowie, L. L., Hu, E. M., et al. 2004, *AJ*, 127, 180
- Capellari, M., Bacon, R., Bureau, M., et al. 2006, *MNRAS*, 366, 1126
- Carleton, N. P., Elvis, M., Fabbiano, G., et al. 1987, *ApJ*, 318, 595
- Chabrier, G. 2003, *PASP*, 115, 763
- Chapman, S. C., Blain, A. W., Smail, I., & Ivison, R. J. 2005, *ApJ*, 622, 772
- Chapman, S. C., Ivison, R. J., Roseboom, I. G., et al. 2010, *MNRAS*, 409, L13
- Chapman, S. C., Smail, I., Windhorst, R., Muxlow, T., & Ivison, R. J. 2004, *ApJ*, 611, 732
- Clements, D., Eales, S., Wojciechowski, K., et al. 2004, *MNRAS*, 351, 447
- Code, A. D., Meade, M. R., Anderson, C. M., et al. 1993, *ApJ*, 403, L63
- Cole, S., Norberg, P., Baugh, C. M., et al. 2001, *MNRAS*, 326, 255
- Conroy, C., Gunn, J. E., & White, M. 2009, *ApJ*, 699, 486
- Coppin, K., Chapin, E. L., Mortier, A. M. J., et al. 2006, *MNRAS*, 372, 1621
- Coppin, K., Swinbank, A. M., Neri, R., et al. 2008, *MNRAS*, 389, 45
- Croton, D., Farrar, G. R., Norberg, P., et al. 2005, *MNRAS*, 356, 1155
- Daddi, E., Cimatti, A., Renzini, A., et al. 2004, *ApJ*, 600, L127
- Davé, R., Finlator, K., Oppenheimer, B. D., et al. 2010, *MNRAS*, 404, 1355
- Devriendt, J. E. G., & Guiderdoni, B. 2000, *A&A*, 363, 851
- Di Matteo, T., Springel, V., & Hernquist, L. 2005, *Nature*, 433, 604
- Donley, J. L., Rieke, G. H., Pérez-González, P. G., & Barro, G. 2008, *ApJ*, 687, 111
- Dye, S. 2008, *MNRAS*, 389, 1293
- Dye, S., Eales, S., Aretxaga, I., et al. 2008, *MNRAS*, 386, 1107
- Eales, S., Lilly, S. J., Gear, W., et al. 1999, *ApJ*, 515, 518
- Eales, S. A., Bertoldi, F., Ivison, R., et al. 2003, *MNRAS*, 344, 169
- Edelson, R. A., & Malkan, M. A. 1986, *ApJ*, 308, 59
- Edelson, R. A., Malkan, M. A., & Rieke, G. 1987, *ApJ*, 321, 233
- Elvis, M., Wilkes, B. J., McDowell, J. C., et al. 1994, *ApJS*, 95, 1
- Erb, D. K., Shapley, A. E., Pettini, M., et al. 2006, *ApJ*, 644, 813
- Erb, D. K., Steidel, C. C., Shapley, A. E., et al. 2006, *ApJ*, 646, 107
- Fitzpatrick, E. L. 1986, *AJ*, 92, 1068
- Flagey, N., Boulanger, F., Verstraete, L., et al. 2006, *A&A*, 453, 969
- Fomalont, E., Kellermann, K. I., Cowie, L. L., et al. 2006, *ApJS*, 167, 103
- Franx, M., Labbé, I., Rudnick, G., et al. 2003, *ApJ*, 587, L79
- Frayser, D. T., Ivison, R. J., Scoville, N. Z., et al. 1998, *ApJ*, 506, L7
- Frayser, D. T., Koda, J., Pope, A., et al. 2008, *ApJ*, 680, L21
- Gallagher, S. C., Richards, G. T., Lacy, M., et al. 2007, *ApJ*, 661, 30
- Gerhard, O., Kronawitter, A., Saglia, R. P., & Bender, R. 2001, *AJ*, 121, 1936
- Glazebrook, K., Abraham, R. G., McCarthy, P. J., et al. 2004, *Nature*, 430, 181
- Greve, T. R., Bertoldi, F., Smail, I., et al. 2005, *MNRAS*, 359, 1165
- Grimes, J. P., Kriss, G. A., & Espey, B. R. 1999, *ApJ*, 526, 130
- Guiderdoni, B., Hivon, E., Bouchet, F. R., & Maffei, B. 1998, *MNRAS*, 295, 877
- Hainline, L. J. 2008, Ph. D. Thesis, California Institute of Technology
- Hainline, L. J., Blain, A. W., Greve, T. R., et al. 2006, *ApJ*, 650, 614
- Hainline, L. J., Blain, A. W., Smail, I., et al. 2009, *ApJ*, 699, 1610 (Paper I)
- Hinshaw, G., Weiland, J. L., Hill, R. S., et al. 2009, *ApJS*, 180, 225
- Hughes, D., Serjeant, S., Dunlop, J., et al. 1998, *Nature*, 394, 241
- Ivison, R. J., Greve, T. R., Smail, I., et al. 2002, *MNRAS*, 337, 1
- Ivison, R. J., Smail, I., Dunlop, J. S., et al. 2005, *MNRAS*, 364, 1025
- Kassin, S. A., de Jong, R. S., & Weiner, B. J. 2006, *ApJ*, 643, 804
- Kauffmann, G., & Charlot, S. 1998, *MNRAS*, 294, 705
- Kauffmann, G., Heckman, T. M., White, S. D. M., et al. 2003, *MNRAS*, 341, 33
- Kauffmann, G., White, S. D. M., & Guiderdoni, B. 1993, *MNRAS*, 264, 201
- Kaviraj, S., Schawinski, K., Devriendt, J. E. G., et al. 2007, *ApJS*, 173, 619
- Kornei, K. A., Shapley, A. E., Erb, D. K., et al. 2010, *ApJ*, 711, 693
- Kovács, A., Chapman, S. C., Dowell, C. D., Blain, A. W., & Phillips, T. G. 2006, *ApJ*, 650, 592
- Kriek, M., van Dokkum, P. G., Franx, M., et al. 2006, *ApJ*, 645, 44
- Kriek, M., van Dokkum, P. G., Franx, M., et al. 2007, *ApJ*, 669, 776
- Kriek, M., van Dokkum, P. G., Franx, M., et al. 2008, *ApJ*, 677, 219
- Kroupa, P. 2001, *MNRAS*, 322, 231
- Le Floc'h, E., Willmer, C. N. A., Noeske, K., et al. 2007, *ApJ*, 660, L65
- Lilly, S. J., Eales, S. A., Gear, W. K. P., et al. 1999, *ApJ*, 518, 641
- Liu, M. C., & Graham, J. R. 2001, *ApJ*, 557, L31
- Lu, N., Helou, G., Werner, M. W., et al. 2003, *ApJ*, 588, 199
- Magnelli, B., Chary, R. R., Pope, A., et al. 2008, *ApJ*, 681, 258
- Magnelli, B., Lutz, D., Berta, S., et al. 2010, *A&A*, 518, L28
- Malkan, M. A., & Filippenko, A. V. 1983, *ApJ*, 275, 477
- Maraston, C. 2005, *MNRAS*, 362, 799
- Maraston, C., Daddi, E., Renzini, A., et al. 2006, *ApJ*, 652, 85
- Maraston, C., Pforr, J., Renzini, A., et al. 2010, *MNRAS*, 407, 830
- Menéndez-Delmestre, K., Blain, A. W., Smail, I., et al. 2009, *ApJ*, 699, 667
- Mentuch, E., Abraham, R. G., Glazebrook, K., et al. 2009, *ApJ*, 706, 1020
- Merloni, A., Bongiorno, A., Bolzonella, M., et al. 2010, *ApJ*, 708, 137
- Michałowski, M., Hjorth, J., & Watson, D. 2010, *A&A*, 514, 67
- Miller, G. E., & Scalo, J. M. 1979, *ApJS*, 41, 513
- Murray, N., Quataert, E., & Thompson, T. A. 2010, *ApJ*, 709, 191

- Mushotzky, R. F., Winter, L. M., McIntosh, D. H., & Tueller, J. 2008, *ApJ*, 684, L65
- Muzzin, A., Marchesini, D., van Dokkum, P. G., et al. 2009, *ApJ*, 701, 1839
- Neri, R., Genzel, R., Ivison, R. J., et al. 2003, *ApJ*, 597, L113
- Neugebauer, G., Green, R. F., Matthews, K., et al. 1987, *ApJS*, 63, 615
- Papovich, C., Dickinson, M., & Ferguson, H. C. 2001, *ApJ*, 559, 620
- Poggianti, B. M., Bressan, A., & Franceschini, A. 2001, *ApJ*, 550, 195
- Poggianti, B. M., & Wu, H. 2000, *ApJ*, 529, 157
- Polletta, M., Tajer, M., Maraschi, L., et al. 2007, *ApJ*, 663, 81
- Pope, A., Borys, C., Scott, D., et al. 2005, *MNRAS*, 358, 149
- Pope, A., Chary, R. R., Alexander, D. M., et al. 2008, *ApJ*, 675, 1171
- Prévot, M., Lequeux, J., Prévot, L., Maurice, E., & Rocca-Volmerange, B. 1984, *A&A*, 132, 389
- Reddy, N. A., Steidel, C. C., Erb, D. K., Shapley, A. E., & Pettini, M. 2006b, *ApJ*, 653, 1004
- Richards, G. T., Lacy, M., Storrie-Lombardi, L. J., et al. 2006, *ApJS*, 166, 470
- Salpeter, E. E. 1955, *ApJ*, 121, 161
- Sawicki, M., & Yee, H. K. C. 1998, *AJ*, 115, 1329
- Schlegel, D. J., Finkbeiner, D. P., & Davis, M. 1998, *ApJ*, 500, 525
- Sellgren, K., Werner, M. W., & Dinerstein, H. L. 1983, *ApJ*, 271, L13
- Seymour, N., Stern, D., De Breuck, C., et al. 2007, *ApJS*, 171, 353
- Shapley, A. E., Steidel, C. C., Adelberger, K. L., et al. 2001, *ApJ*, 562, 95
- Shapley, A. E., Steidel, C. C., Erb, D. K., et al. 2005, *ApJ*, 626, 698
- Silk, J. 1997, *ApJ*, 481, 703
- Simpson, C., & Rawlings, S. 2000, *MNRAS*, 317, 1023
- Smail, I., Chapman, S. C., Blain, A. W., & Ivison, R. J. 2004, *ApJ*, 616, 71
- Smail, I., Ivison, R. J., & Blain, A. W. 1997, *ApJ*, 490, L5
- Smail, I., Ivison, R. J., Blain, A. W., & Kneib, J.-P. 1998, *ApJ*, 507, L21
- Smail, I., Ivison, R. J., Blain, A. W., & Kneib, J.-P. 2002, *MNRAS*, 331, 495
- Steidel, C. C., Adelberger, K. L., Shapley, A. E., et al. 2003, *ApJ*, 592, 728
- Swinbank, A. M., Chapman, S. C., Smail, I., et al. 2006, *MNRAS*, 371, 465
- Swinbank, A. M., Lacey, C. G., Smail, I., et al. 2008, *MNRAS*, 391, 420
- Swinbank, A. M., Smail, I., Chapman, S. C., et al. 2010, *MNRAS*, 405, 234
- Swinbank, A. M., Smail, I., Chapman, S. C., et al. 2004, *ApJ*, 617, 64
- Tacconi, L. J., Genzel, R., Neri, R., et al. 2010, *Nature*, 463, 781
- Tacconi, L. J., Genzel, R., Smail, I., et al. 2008, *ApJ*, 680, 246
- Tacconi, L. J., Neri, R., Chapman, S. C., et al. 2006, *ApJ*, 640, 228
- Takata, T., Sekiguchi, K., Smail, I., et al. 2006, *ApJ*, 651, 713
- Tecza, M., Baker, A. J., Davies, R. I., et al. 2004, *ApJ*, 605, L109
- van der Wel, A., Franx, M., Wuyts, S., et al. 2006, *ApJ*, 652, 97
- Wardlow, J. L., Smail, I., Coppin, K. E. K., et al. 2011, *MNRAS*, 415, 1479
- Weiß A., Kovács, A., Coppin, K. E. K., et al. 2009, *ApJ*, 707, 1201
- Whitaker, K. E., van Dokkum, P. G., Brammer, G., et al. 2010, *ApJ*, 719, 1715
- Williams, M. J., Bureau, M., & Cappellari, M. 2009, *MNRAS*, 400, 1665

Table 1
Photometric Data Used in SED Fits of C05 SMGs

Field Name	Optical Bands	Near-IR Bands	IRAC Bands (μm)	(# Optical Bands) ^a (per galaxy)	Galactic $E(B-V)$ ^b (mag)
CFRS-03h	U, B, V, R, I	J, K	3.6, 4.5, 5.8, 8.0	6	0.071
Lockman	B, R, I	K	3.6, 4.5, 5.8, 8.0	3	0.007
GOODS-N	U, B, V, R, I, z'	J, K	3.6, 4.5, 5.8, 8.0	8	0.011
SSA-13	B, R, I, z	J, K	3.6, 4.5, 5.8, 8.0	6	0.014
CFRS-14h	B, R, I	J, K	3.6, 4.5, 5.8, 8.0	5	0.011
ELAIS-N2	B, V, R, I	K	3.6, 4.5, 5.8, 8.0	5	0.006
SSA-22	B, R, I	J, K	3.6, 4.5, 5.8, 8.0	5	0.061

^a The median number of optical and near-IR photometric bands per SMG actually used in the SED fits.

^b Estimated line-of-sight reddening due to the Milky Way from Schlegel et al. (1998).

Table 2
Results of SED Fitting and Stellar Masses for C05 Spectroscopic SMG Sample, M05 Models

Chapman et al. (2005) ID	z_{spec}	$M_H(\text{obs})^a$ (mag, Vega)	$M_H(\text{PL-sub})^b$ (mag, Vega)	α^c	PL Fraction (IB) ^d	PL Fraction (CSF) ^e	A_V^f (mag)	$\log M_\star^g$ (M_\odot)
SMM J030227.73+000653.5	1.408	-26.64 \pm 0.16	-26.60 \pm 0.14	3.0	0.8 ^{+0.1} _{-0.1}	0.6 ^{+0.1} _{-0.1}	1.6 \pm 0.4	11.06 \pm 0.08
SMM J030231.81+001031.3	1.316	> -22.22	> -22.11	2.0	0.0 ^{+0.9} _{-0.1}	0.2 ^{+0.3} _{-0.1}	...	< 9.26
SMM J030236.15+000817.1	2.435	-25.91 \pm 0.09	-25.82 \pm 0.09	2.0	0.2 ^{+0.5} _{-0.2}	0.2 ^{+0.5} _{-0.2}	1.6 \pm 0.4	10.74 \pm 0.05
SMM J030238.62+001106.3	0.276 ^h	-25.68 \pm 0.07	-25.68 \pm 0.07	2.0	0.0 ^{+0.3} _{-0.1}	0.0 ^{+0.4} _{-0.1}	1.8 \pm 0.3	10.69 \pm 0.06
SMM J030244.82+000632.3 ⁱ	0.176	> -22.98	> -22.98	2.0	0.0 ^{+0.1} _{-0.1}	0.0 ^{+0.1} _{-0.1}	...	< 9.61
SMM J105151.69+572636.0	1.620	-27.34 \pm 0.02	-26.83 \pm 0.23	2.0	0.5 ^{+0.1} _{-0.5}	0.2 ^{+0.1} _{-0.2}	1.0 \pm 1.0	11.16 \pm 0.11
SMM J105155.47+572312.7	2.686	-25.71 \pm 0.08	-25.13 \pm 0.08	3.0	0.8 ^{+0.1} _{-0.1}	0.7 ^{+0.1} _{-0.1}	0.3 \pm 0.3	10.47 \pm 0.05
SMM J105158.02+571800.2	2.694	-27.24 \pm 0.08	-27.24 \pm 0.08	2.0	0.0 ^{+0.2} _{-0.2}	0.0 ^{+0.1} _{-0.1}	1.3 \pm 0.4	11.31 \pm 0.05
SMM J105200.22+572420.2	0.689	-23.88 \pm 0.14	-23.48 \pm 0.08	3.0	1.0 ^{+0.1} _{-0.1}	1.0 ^{+0.1} _{-0.1}	1.0 \pm 0.4	9.81 \pm 0.05
SMM J105201.25+572445.7	2.148	-25.56 \pm 0.04	-24.96 \pm 0.06	3.0	0.7 ^{+0.1} _{-0.1}	0.7 ^{+0.1} _{-0.1}	1.4 \pm 0.1	10.40 \pm 0.04
SMM J105207.49+571904.0	2.689	> -26.29	> -26.29	2.0	0.0 ^{+0.6} _{-0.2}	0.0 ^{+0.5} _{-0.1}	1.8 \pm 0.3	< 10.93
SMM J105219.15+571858.4	2.372	-26.28 \pm 0.01	-26.28 \pm 0.01	2.0	0.0 ^{+0.4} _{-0.1}	0.0 ^{+0.4} _{-0.1}	1.5 \pm 0.0	10.93 \pm 0.05
SMM J105227.58+572512.4	2.470	-27.08 \pm 0.06	-27.06 \pm 0.04	3.0	0.1 ^{+0.2} _{-0.1}	0.0 ^{+0.3} _{-0.1}	1.8 \pm 0.3	11.24 \pm 0.04
SMM J105227.77+572218.2	1.956	> -23.32	> -23.11	3.0	0.5 ^{+0.4} _{-0.3}	0.5 ^{+0.4} _{-0.3}	...	< 9.66
SMM J105230.73+572209.5	2.611	-27.38 \pm 0.08	-27.31 \pm 0.11	3.0	0.1 ^{+0.3} _{-0.1}	0.3 ^{+0.2} _{-0.3}	1.0 \pm 0.4	11.34 \pm 0.05
SMM J105238.19+571651.1	1.852	-25.39 \pm 0.08	-25.38 \pm 0.07	3.0	0.1 ^{+0.5} _{-0.1}	0.0 ^{+0.7} _{-0.3}	0.4 \pm 0.4	10.57 \pm 0.05
SMM J105238.30+572435.8	3.036	-27.31 \pm 0.12	-27.31 \pm 0.12	2.0	0.0 ^{+0.1} _{-0.1}	0.0 ^{+0.1} _{-0.1}	2.1 \pm 0.3	11.34 \pm 0.08
SMM J123549.44+621536.8	2.203	-27.13 \pm 0.15	-26.92 \pm 0.21	3.0	0.8 ^{+0.1} _{-0.8}	0.0 ^{+0.9} _{-0.1}	1.0 \pm 0.2	11.20 \pm 0.11
SMM J123553.26+621337.7 ^j	2.098	-25.74 \pm 0.12	-25.31 \pm 0.02	3.0	0.7 ^{+0.2} _{-0.2}	0.8 ^{+0.1} _{-0.1}	1.2 \pm 0.0	10.54 \pm 0.05
SMM J123555.14+620901.7 ^j	1.875	-27.11 \pm 0.05	-26.76 \pm 0.03	3.0	0.8 ^{+0.1} _{-0.1}	0.7 ^{+0.1} _{-0.1}	1.8 \pm 0.0	11.12 \pm 0.05
SMM J123600.15+621047.2	1.994	-26.02 \pm 0.13	-24.69 \pm 0.09	3.0	0.9 ^{+0.1} _{-0.1}	0.9 ^{+0.1} _{-0.1}	3.0 \pm 0.3	10.30 \pm 0.07
SMM J123606.72+621550.7	2.416	-25.94 \pm 0.03	-25.01 \pm 0.04	2.0	0.8 ^{+0.1} _{-0.1}	0.8 ^{+0.1} _{-0.1}	0.3 \pm 0.0	10.42 \pm 0.05
SMM J123606.85+621021.4	2.509	-26.95 \pm 0.01	-26.95 \pm 0.01	2.0	0.0 ^{+0.3} _{-0.1}	0.0 ^{+0.2} _{-0.1}	1.8 \pm 0.0	11.20 \pm 0.05
SMM J123616.15+621513.7	2.578	-26.91 \pm 0.01	-25.84 \pm 0.73	2.0	0.9 ^{+0.1} _{-0.9}	0.6 ^{+0.2} _{-0.2}	1.4 \pm 1.4	10.85 \pm 0.27
SMM J123618.33+621550.5	2.000	-25.85 \pm 0.07	-25.75 \pm 0.07	3.0	0.5 ^{+0.5} _{-0.5}	0.5 ^{+0.5} _{-0.4}	1.3 \pm 0.4	10.71 \pm 0.05
SMM J123621.27+621708.4	1.988	-25.77 \pm 0.03	-25.64 \pm 0.08	3.0	0.4 ^{+0.1} _{-0.4}	0.5 ^{+0.3} _{-0.2}	1.0 \pm 0.4	10.67 \pm 0.05
SMM J123622.65+621629.7	2.466	-26.84 \pm 0.05	-26.73 \pm 0.10	3.0	0.2 ^{+0.3} _{-0.3}	0.3 ^{+0.2} _{-0.2}	1.3 \pm 0.4	11.11 \pm 0.05
SMM J123629.13+621045.8	1.013	-26.42 \pm 0.04	-26.37 \pm 0.04	2.0	0.5 ^{+0.1} _{-0.2}	0.6 ^{+0.1} _{-0.3}	3.3 \pm 0.3	10.96 \pm 0.04
SMM J123632.61+620800.1 ^j	1.993	-26.30 \pm 0.10	-24.97 \pm 0.09	3.0	0.9 ^{+0.1} _{-0.1}	0.9 ^{+0.1} _{-0.1}	1.2 \pm 0.3	10.41 \pm 0.07
SMM J123634.51+621241.0	1.219	-26.29 \pm 0.07	-26.02 \pm 0.06	3.0	0.7 ^{+0.1} _{-0.4}	0.8 ^{+0.1} _{-0.1}	1.5 \pm 0.3	10.82 \pm 0.04
SMM J123635.59+621424.1 ^j	2.005	-27.90 \pm 0.14	-27.16 \pm 0.19	3.0	0.9 ^{+0.1} _{-0.1}	0.8 ^{+0.1} _{-0.1}	2.2 \pm 0.5	11.29 \pm 0.10
SMM J123636.75+621156.1	0.557	-23.54 \pm 0.04	-23.52 \pm 0.05	2.0	0.7 ^{+0.1} _{-0.3}	0.6 ^{+0.2} _{-0.6}	1.8 \pm 0.0	9.83 \pm 0.06
SMM J123707.21+621408.1	2.484	-26.93 \pm 0.01	-26.93 \pm 0.01	2.0	0.0 ^{+0.4} _{-0.1}	0.0 ^{+0.3} _{-0.1}	2.4 \pm 0.0	11.19 \pm 0.05
SMM J123711.98+621325.7	1.992	-25.25 \pm 0.07	-25.15 \pm 0.08	3.0	0.4 ^{+0.3} _{-0.4}	0.5 ^{+0.2} _{-0.4}	1.3 \pm 0.4	10.47 \pm 0.05
SMM J123712.05+621212.3	2.914	-26.94 \pm 0.07	-26.94 \pm 0.07	2.0	0.0 ^{+0.7} _{-0.1}	0.0 ^{+0.5} _{-0.1}	2.5 \pm 0.5	11.19 \pm 0.05
SMM J123721.87+621035.3	0.979	-25.88 \pm 0.03	-25.80 \pm 0.01	2.0	0.6 ^{+0.2} _{-0.2}	0.5 ^{+0.2} _{-0.4}	2.1 \pm 0.0	10.74 \pm 0.05
SMM J131201.17+424208.1	3.405	-27.11 \pm 0.06	-26.37 \pm 0.07	3.0	0.5 ^{+0.1} _{-0.3}	0.5 ^{+0.1} _{-0.3}	0.6 \pm 0.3	10.96 \pm 0.04
SMM J131208.82+424129.1	1.544	-26.15 \pm 0.03	-26.11 \pm 0.07	3.0	0.5 ^{+0.1} _{-0.3}	0.0 ^{+0.3} _{-0.3}	2.4 \pm 0.3	10.86 \pm 0.06
SMM J131212.69+424422.5	2.805	> -25.74	> -25.69	3.0	0.2 ^{+0.6} _{-0.2}	0.0 ^{+0.6} _{-0.1}	1.8 \pm 0.3	< 10.70
SMM J131215.27+423900.9 ^k	2.565	-29.49 \pm 0.07	-28.75 \pm 0.03	3.0	0.7 ^{+0.1} _{-0.4}	0.8 ^{+0.1} _{-0.1}	0.2 \pm 0.2	11.92 \pm 0.04
SMM J131222.35+423814.1	2.565	-28.32 \pm 0.10	-27.34 \pm 0.18	3.0	0.9 ^{+0.1} _{-0.1}	0.8 ^{+0.1} _{-0.1}	0.4 \pm 0.4	11.36 \pm 0.10
SMM J131225.20+424344.5	1.038	-25.73 \pm 0.04	-25.60 \pm 0.04	3.0	0.8 ^{+0.1} _{-0.1}	0.8 ^{+0.1} _{-0.4}	1.4 \pm 0.1	10.66 \pm 0.04
SMM J131225.73+423941.4	1.554	-25.25 \pm 0.10	-25.25 \pm 0.10	2.0	0.0 ^{+0.5} _{-0.1}	0.0 ^{+0.6} _{-0.6}	1.0 \pm 0.4	10.52 \pm 0.05
SMM J131228.30+424454.8	2.931	-26.65 \pm 0.02	-26.14 \pm 0.10	3.0	0.6 ^{+0.1} _{-0.2}	0.7 ^{+0.1} _{-0.2}	1.2 \pm 0.0	10.87 \pm 0.05
SMM J131232.31+423949.5	2.320	-27.68 \pm 0.01	-24.31 \pm 0.03	2.0	1.0 ^{+0.1} _{-0.1}	1.0 ^{+0.1} _{-0.1}	4.8 \pm 0.0	10.14 \pm 0.05
SMM J131239.14+424155.7	2.242	-25.44 \pm 0.06	-25.41 \pm 0.09	2.0	0.0 ^{+0.3} _{-0.1}	0.2 ^{+0.5} _{-0.2}	1.3 \pm 0.4	10.58 \pm 0.05
SMM J141741.81+522823.0	1.150	-28.53 \pm 0.06	-28.12 \pm 0.09	3.0	0.9 ^{+0.1} _{-0.1}	0.9 ^{+0.1} _{-0.1}	2.8 \pm 0.4	11.67 \pm 0.07

Table 2 — Continued

Chapman et al. (2005) ID	z_{spec}	$M_H(\text{obs})^a$ (mag, Vega)	$M_H(\text{PL-sub})^b$ (mag, Vega)	α^c	PL Fraction (IB) ^d	PL Fraction (CSF) ^e	A_V^f (mag)	$\log M_\star^g$ (M_\odot)
SMM J141742.04+523025.7	0.661	-25.66 ± 0.15	-25.49 ± 0.15	2.0	$0.8^{+0.1}_{-0.1}$	$0.8^{+0.1}_{-0.1}$	0.6 ± 0.3	10.62 ± 0.09
SMM J141750.50+523101.0	2.128	> -23.65	> -23.65	2.0	$0.0^{+0.5}_{-0.5}$	$0.0^{+0.3}_{-0.3}$...	< 9.88
SMM J141800.40+522820.3	1.913	-26.67 ± 0.09	-26.56 ± 0.10	3.0	$0.5^{+0.1}_{-0.2}$	$0.4^{+0.2}_{-0.2}$	1.8 ± 0.3	11.05 ± 0.07
SMM J141802.87+523011.1	2.127	-24.30 ± 0.01	-24.27 ± 0.02	3.0	$0.3^{+0.5}_{-0.3}$	$0.0^{+0.3}_{-0.3}$	0.2 ± 0.2	10.12 ± 0.05
SMM J141809.00+522803.8	2.712	-27.79 ± 0.05	-27.79 ± 0.05	2.0	$0.0^{+0.1}_{-0.1}$	$0.0^{+0.1}_{-0.1}$	2.1 ± 0.3	11.53 ± 0.04
SMM J141813.54+522923.4	3.484	> -25.38	> -25.32	2.0	$0.7^{+0.2}_{-0.7}$	$0.7^{+0.1}_{-0.6}$...	< 10.55
SMM J163627.94+405811.2	3.180	> -25.17	> -24.68	2.0	$0.7^{+0.1}_{-0.5}$	$0.5^{+0.2}_{-0.5}$	0.3 ± 0.3	< 10.30
SMM J163631.47+405546.9	2.283	-26.19 ± 0.07	-25.84 ± 0.09	2.0	$0.6^{+0.1}_{-0.3}$	$0.6^{+0.1}_{-0.2}$	1.0 ± 0.4	10.75 ± 0.05
SMM J163639.01+405635.9	1.495	-25.74 ± 0.06	-25.43 ± 0.11	3.0	$0.9^{+0.1}_{-0.2}$	$0.7^{+0.1}_{-0.2}$	1.5 ± 0.6	10.59 ± 0.07
SMM J163650.43+405734.5	2.378	-27.07 ± 0.08	-26.39 ± 0.28	2.0	$0.8^{+0.1}_{-0.3}$	$0.6^{+0.1}_{-0.4}$	0.6 ± 0.3	10.99 ± 0.13
SMM J163658.19+410523.8	2.454	-26.61 ± 0.08	-26.48 ± 0.09	2.0	$0.2^{+0.3}_{-0.2}$	$0.3^{+0.3}_{-0.3}$	1.6 ± 0.4	11.01 ± 0.05
SMM J163658.78+405728.1	1.190	-26.22 ± 0.06	-26.17 ± 0.08	3.0	$0.7^{+0.1}_{-0.1}$	$0.4^{+0.3}_{-0.2}$	2.1 ± 0.3	10.89 ± 0.06
SMM J163704.34+410530.3	0.840	-23.57 ± 0.12	-23.46 ± 0.23	2.0	$0.8^{+0.1}_{-0.2}$	$0.0^{+0.8}_{-0.8}$	1.3 ± 0.4	9.81 ± 0.11
SMM J163706.51+405313.8	2.374	-27.08 ± 0.14	-26.76 ± 0.21	3.0	$0.7^{+0.1}_{-0.2}$	$0.4^{+0.1}_{-0.3}$	2.1 ± 0.3	11.13 ± 0.11
SMM J221733.12+001120.2	0.652	-25.60 ± 0.10	-25.53 ± 0.04	3.0	$0.6^{+0.1}_{-0.2}$	$0.7^{+0.1}_{-0.2}$	1.8 ± 0.0	10.63 ± 0.05
SMM J221733.91+001352.1	2.865	-26.85 ± 0.07	-26.49 ± 0.04	3.0	$0.6^{+0.1}_{-0.2}$	$0.3^{+0.2}_{-0.2}$	0.9 ± 0.3	11.01 ± 0.05
SMM J221735.15+001537.2	3.098	-25.71 ± 0.07	-25.22 ± 0.18	3.0	$0.3^{+0.2}_{-0.3}$	$0.4^{+0.2}_{-0.3}$	0.8 ± 0.5	10.51 ± 0.07
SMM J221735.84+001558.9	3.089	-26.20 ± 0.01	-25.79 ± 0.20	2.0	$0.6^{+0.1}_{-0.4}$	$0.3^{+0.3}_{-0.3}$	1.2 ± 0.3	10.74 ± 0.10
SMM J221804.42+002154.4	2.517	-26.18 ± 0.01	-25.92 ± 0.03	3.0	$0.6^{+0.1}_{-0.6}$	$0.5^{+0.3}_{-0.5}$	1.2 ± 0.0	10.79 ± 0.05
SMM J221806.77+001245.7	1.910	-26.17 ± 0.09	-26.17 ± 0.09	2.0	$0.0^{+0.1}_{-0.1}$	$0.0^{+0.1}_{-0.1}$	2.1 ± 0.3	10.89 ± 0.07

^a Absolute rest-frame H magnitude derived from observed photometry, averaged between instantaneous burst and continuous SFH model fits.

^b Absolute rest-frame H magnitude when best-fit PL fraction is subtracted, averaged between instantaneous burst and continuous SFH model fits.

^c Choice of PL index resulting in best fit for galaxy (lowest χ^2_ν). In the cases where the best-fit PL fraction is zero, the value listed in this column indicates the index for which the error bar is calculated.

^d Best-fit fraction of observed $8.0 \mu\text{m}$ flux contributed by PL component for instantaneous burst SFH models.

^e Best-fit fraction of observed $8.0 \mu\text{m}$ flux contributed by PL component for continuous SFH models.

^f Average of best-fit V -band extinctions from instantaneous burst and continuous SFH fits. The listed error is calculated as half the difference between the two averaged values.

^g Stellar mass derived as described in §3.2. The listed error represents half the difference between the instantaneous burst and continuous SFH values.

^h SED fits indicate that C05 redshift of $z = 0.276$ is incorrect. Photometric redshift obtained from HYPER-Z suggests alternate redshift of $z = 1.81$. M_\star has been calculated using $z = 1.81$. Due to uncertainty in the redshift, the results derived for this galaxy have not been included in the analysis here.

ⁱ SED fitting fails to converge for any model, possibly due to incorrect galaxy redshift or error in counterpart selection when measuring optical and IRAC photometry. The results for this galaxy have not been included in any of the analysis in the text.

^j SMG displays UV/blue excess.

^k Known optical QSO.

Table 3
Near-IR Continuum Excess-Dominated SMGs^a

Chapman et al. (2005) ID	% L_H in PL Component (IB)	% L_H in PL Component (CSF)
SMM J123600.15+621047.2 ^b	67	68
SMM J123606.72+621550.7	56	56
SMM J123616.15+621513.7	71	35
SMM J123632.61+620800.1 ^c	67	67
SMM J131215.27+423900.9	45	51
SMM J131222.35+423814.1	60	54
SMM J131232.31+423949.5	97	97
SMM J163650.43+405734.5	53	28

^a "Continuum-Dominated" is defined as having greater than 50% of the total L_H contributed by the PL component.

^b Possible Compton-thick AGN; see Fig. 4 of Alexander et al. (2008b).

^c SMG displays UV/blue excess.

Table 4
SMGs with CO Observations

Chapman et al. (2005) ID	z_{spec}	CO Transition	$M(\text{H}_2)^a$ $\times 10^{10} M_\odot$	M_{dyn} $\times 10^{11} M_\odot$	Reference
SMM J105230.73+572209.5	2.611	3 \rightarrow 2	< 1.4	...	1
SMM J105238.30+572435.8	3.036	3 \rightarrow 2	< 3.0	...	1
SMM J123549.44+621536.8	2.202	3 \rightarrow 2	3.2	0.94	2
SMM J123618.33+621550.5	2.000	4 \rightarrow 3	7.2	2.2	3
SMM J123634.51+621241.0	1.219	2 \rightarrow 1	6.8	7.0	4
SMM J123707.21+621408.1	2.490	3 \rightarrow 2	2.3	2.4	2
SMM J123711.98+621325.7	1.992	4 \rightarrow 3	3.5	...	3
SMM J131201.17+424208.1	3.405	1 \rightarrow 0	16	1.2	1,5
SMM J131222.35+423814.1	2.565	3 \rightarrow 2	1.0	0.25	6
SMM J131232.31+423949.5	2.320	3 \rightarrow 2	< 2.4	...	1
SMM J163631.47+405546.9	2.283	3 \rightarrow 2	< 0.9	...	1
SMM J163639.01+405635.9	1.495	2 \rightarrow 1	< 1.8	...	1
SMM J163650.43+405734.5	2.380	3 \rightarrow 2	5.4	3.4	2
SMM J163658.19+410523.8	2.454	3 \rightarrow 2	4.4	1.4	2
SMM J163706.51+405313.8	2.374	3 \rightarrow 2	2.4	3.4	1
SMM J221735.15+001537.2	3.098	3 \rightarrow 2	3.0	2.8	1

Note. — References: (1) Greve et al. (2005); (2) Tacconi et al. (2008); (3) Bothwell et al. (2010); (4) Frayer et al. (2008); (5) Hainline et al. (2006); (6) Coppin et al. (2008)

^a $M(\text{H}_2)$ calculated assuming a CO-to- H_2 conversion factor $\alpha = 0.8$ and $L'_{\text{CO}(4\rightarrow3)}/L'_{\text{CO}(1\rightarrow0)} = 1.0$, $L'_{\text{CO}(3\rightarrow2)}/L'_{\text{CO}(1\rightarrow0)} = 1.0$, or $L'_{\text{CO}(2\rightarrow1)}/L'_{\text{CO}(1\rightarrow0)} = 1.0$.